Positron emission particle tracking (PEPT): A novel approach to flow visualisation in lab-scale anaerobic digesters

Article *in* Flow Measurement and Instrumentation · February 2017

DOI: 10.1016/j.flowmeasinst.2017.02.009

CITATIONS
18

READS
106

4 authors, including:

Rebecca C. Sindall
RNLI
31 PUBLICATIONS **197** CITATIONS
SEE PROFILE

Davide Dapelo
University of Liverpool
18 PUBLICATIONS **337** CITATIONS
SEE PROFILE

John Bridgeman
University of Liverpool
104 PUBLICATIONS **3,310** CITATIONS
SEE PROFILE

Positron emission particle tracking (PEPT): A novel approach to flow visualisation in lab-scale anaerobic digesters

Rebecca C. Sindall, Davide Dapelo, Tom Leadbeater, John Bridgeman

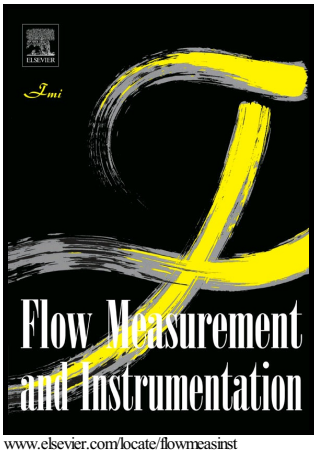

www.elsevier.com/locate/flowmeasinst

PII: S0955-5986(17)30051-1
DOI: http://dx.doi.org/10.1016/j.flowmeasinst.2017.02.009
Reference: JFMI1322

To appear in: *Flow Measurement and Instrumentation*

Received date: 21 May 2016
Revised date: 18 October 2016
Accepted date: 5 February 2017

Cite this article as: Rebecca C. Sindall, Davide Dapelo, Tom Leadbeater and John Bridgeman, Positron emission particle tracking (PEPT): A novel approach to flow visualisation in lab-scale anaerobic digesters, *Flow Measurement and Instrumentation,* http://dx.doi.org/10.1016/j.flowmeasinst.2017.02.009

Positron emission particle tracking (PEPT): A novel approach to flow visualisation in lab-scale anaerobic digesters

Rebecca C Sindall[1], Davide Dapelo[1*], Tom Leadbeater[2], John Bridgeman[1]

[1]Department of Civil Engineering, University of Birmingham

[2]Department of Physics, University of Cape Town

[*]Corresponding author. dapelod@bham.ac.uk

Abstract

Positron emission particle tracking (PEPT) was used to visualise the flow patterns established by mixing in two laboratory-scale anaerobic digesters fitted with mechanical mixing or gas mixing apparatus. PEPT allows the visualisation of flow patterns within a digester without necessitating the use of a transparent synthetic sludge. In the case of the mechanically-mixed digester, the mixing characteristics of opaque sewage sludge was compared to a transparent synthetic sludge at different mixing speeds. In the gas-mixed apparatus, two synthetic sludges were compared. In all scenarios, quasi-toroidal flow paths were established. However, mixing was less successful in more viscous liquids unless mixing power was increased to compensate for the increase in viscosity. The robustness of the PEPT derived velocities was found to be significantly affected by the frequency with which the particle enters a given volume of the vessel, with the accuracy of the calculated velocity decreasing in regions with low data capture. Nevertheless, PEPT was found to offer a means of accurate validation of computational fluid dynamics models which in turn can help to optimise flow patterns for biogas production.

Keywords: anaerobic digestion; mechanical mixing; gas mixing; flow patterns; particle tracking

1. Introduction

Anaerobic digestion (AD) is widely used for sustainable energy production, in the form of biogas, and management of sludge from wastewater treatment plants as well as municipal solid waste and livestock facilities. Mixing enables a uniform distribution of nutrients to micro-organisms, facilitates the generation of a methane-rich biogas for use as a valuable renewable energy source, and when performed correctly prevents the settlement of heavier particles (Ward et al., 2008). However, mixing is an energy intensive operation and can range from 10 to 100 W h^{-1} m^{-3}, depending on the digester design, the mixing method and the total solids in the feedstock (Burton and Turner, 2003). Mixing is generally effected via mechanical agitation using an impeller, or gas injection. Gas mixing takes biogas from the top of the digester and pumps it into the sludge at the base of the digester through a series of nozzles. As the bubbles rise, the momentum transfer to the surrounding sludge causes mixing.

Because of the importance of effective mixing, there is a growing body of research, both using traditional flow visualisation techniques (Hoffman et al., 2008) and, more commonly, computational fluid dynamics (CFD) (Bridgeman, 2012; Sindall et al., 2013; Wu, 2010; Wu, 2012), that aims to determine the optimum mixing conditions for digestion. Optimum mixing conditions would minimise the cost of mixing whilst maximising the production of biogas from the digester. The difficulty of performing investigations on operational industrial-scale digesters, has in the majority of cases limited the research to laboratory-scale designs. The outcome of laboratory-scale research has been used to give recommendations to be applied at full-scale. In the case of CFD research, it is common to validate a computational model against a lab-scale setup (Wu, 2010, Dapelo et al., 2015, Dapelo and Bridgeman, 2015), and then apply the validated model to a full-scale design. The optimisation of mixing processes in AD is further complicated by the intrinsic properties of sludge. First, sludge displays complex non-Newtonian characteristics such as shear thinning, yield stress and shear banding (Baudez et al., 2013), and it is well-known that Newtonian and non-Newtonian fluids behave differently in a stirred tank (Holland and Chapman, 1966). Secondly, sludge is opaque. This means that optical flow visualization techniques, such as particle image velocimetry (PIV) and laser Doppler anemometry (LDA), that are often applied to transparent solutions cannot be applied to sludge. Attempts to overcome this by using a transparent synthetic sludge have not been completely successful; for example, when reproducing gas mixing, Dapelo et al. (2015) observed difficulty in measuring the continuous phase velocity field in proximity to a lab-scale bubble column with PIV due to the refraction effect of the bubbles on the laser beams.

Positron Emission Particle Tracking (PEPT) is a technique, developed at the University of Birmingham, which allows a radioactive tracer particle to be tracked (Parker et al., 1993). Since its development, PEPT has been used to visualise fluid flow in a wide range of opaque vessels from heat exchangers (Bakalis et al., 2006) to dishwashers (Perez-Mohedano et al., 2015). It has been shown to be a successful visualisation technique for a wide range of mixing problems such as turbulent mixing of fluids (Chiti et al., 2011), including those with non-Newtonian rheology (Fangary et al. 2000; Bakalis et al., 2004); mixing of solid-liquid suspensions and slurries; granular and particulate material mixing; (Leadbeater et al., 2012), and multi-phase flows (Pianko-Oprych et al., 2009). This ability to visualize flow patterns in complex systems offers significant advantages over traditional flow visualisation techniques, such as PIV, including for the validation of CFD models (Barigou, 2004). The technique is particularly promising for application in AD as it is unaffected by the optical properties of the liquid phase. As such, it can provide reliable data without the need for a transparent synthetic sludge and can additionally provide data for the movement of fluid close to the bubble column.

This paper considers the application of the PEPT technique to lab-scale anaerobic digesters with both impeller mixing and gas mixing in order to identify flow patterns. The application of PEPT within an opaque sewage sludge offers an opportunity to accurately validate CFD models and further the optimisation of mixing regimes to maximise biogas production for use as a renewable energy source. The flow patterns in the mechanically-mixed and gas-mixed vessels are compared and the effects of viscosity on those flow patterns are demonstrated. Additionally, the benefits and limitations of the PEPT technique are compared to PIV.

2. Theory

2.1. PEPT

The PEPT technique, developed at University of Birmingham, is based on the medical imaging technique, Positron Emission Tomography (PET), where the spatial distribution of radioactive material is measured by detecting the gamma emissions produced by radioactive decay. In PEPT, however, rather than a volume of activity being imaged, a single particle is labelled with a proton-rich isotope and all gamma ray emissions are then assumed to originate from this particle. This allows the neutrally buoyant particle to be tracked as it moves through the liquid phase, so representing a flow follower or liquid volume element.

For these isotopes, positrons are produced by β^+ decay, and then quickly annihilate with local electrons in the surrounding media. This annihilation results in a pair of gamma photons which are constrained to have equal and opposite momenta, i.e. they are produced travelling at 180°. Provided both photons are detected, the line along which they travel can be reconstructed, with the annihilation site placed somewhere along this Line of Response (LoR). In PEPT, a set of consecutive LoRs are recorded on a rapid timescale and a triangulation technique is applied to locate the centroid of the LoR ensemble; this is assumed to be the instantaneous particle position. This technique has been shown to locate particles through a significant number of dense and opaque materials and is relatively insensitive to the effects of gamma ray scatter and attenuation. Typically, at Birmingham, LoRs can be acquired at rates up to 100 kHz, giving particle location rates of around 1 kHz which are accurate to around 0.5 mm in three dimensions.

2.2. Calculation of velocity field

The output of a PEPT run is a succession:

$$(\vec{x}_n^{tr}, t_n), n = 1, \dots, N, \qquad \text{Equation 1}$$

where $\vec{x}_n^{tr} \equiv (x_n^{tr}, y_n^{tr}, z_n^{tr})$ are the measured Cartesian coordinates of the tracer particle at the time t_n, and the integer n labels the time step. An averaged Eulerian liquid velocity field $\vec{u}(\vec{x})$ was calculated from the PEPT measurements (Equation 1). A succession for the velocities:

$$(\vec{u}_n^{tr}, t_n), n = 2, \dots, N-1, \qquad \text{Equation 2}$$

can be determined from the PEPT output (Equation 1) by applying a central differencing scheme:

$$\vec{u}_n^{tr} \approx \frac{|\vec{x}_n^{tr} - \vec{x}_{n-1}^{tr}| + |\vec{x}_{n+1}^{tr} - \vec{x}_n^{tr}|}{t_{n+1} - t_{n-1}} \qquad \text{Equation 3}$$

Higher order differencing schemes may be in principle more appropriate than the central scheme due to the reduced sensitivity to fluctuations affecting two contiguous points. This problem arises when the measurement spatial resolution is as large as, or bigger than the distance between two contiguous samplings. This situation occurred in the gas-mixed measurements. Instead of adopting higher order schemes, an equivalent solution was found

by applying a moving average filter to the tracer positions (Equation 1) before computing the velocity in the gas-mixed measurements. In this way, each data point was replaced with the average between that point and the preceding four points.

The Eulerian velocity field was found to be axis-symmetric (see Section 4). Therefore, the information regarding $\vec{u}(\vec{x})$ reduces to a knowledge of $\vec{u}(r,\, y)$. The domain $(0,\, R) \times (0,\, H)$ can be decomposed into small rectangles, each labelled by the integers $(\alpha,\, \beta)$, by dividing the interval $(0,\, R)$ into N_r parts, and $(0,\, H)$ into N_y parts. Therefore we have $\alpha = 1, \dots, N_r$ and $= 1, \dots, N_y$. $\vec{u}(r,\, y)$ is then approximated by $\vec{u}_{\alpha\beta}$, that takes a constant value inside the rectangle $(\alpha,\, \beta)$.

The PEPT output (Equation 1) can therefore be converted into a discretized form:

$$(\alpha_n,\, \beta_n,\, t_n)\,, \qquad n = 1, \dots, N \qquad \text{Equation 5}$$

by using the following :

$$\begin{aligned} \alpha_n &= \mathrm{int}\left[r_n^{\mathrm{tr}}\, \frac{N_r}{R} - \varepsilon\right] + 1 \\ \beta_n &= \mathrm{int}\left[y_n^{\mathrm{tr}}\, \frac{N_y}{H} - \varepsilon\right] + 1\,, \end{aligned} \qquad \text{Equation 6}$$

where:

$$r_n^{\mathrm{tr}} = \sqrt{(x_n^{\mathrm{tr}})^2 + (z_n^{\mathrm{tr}})^2}\ . \qquad \text{Equation 7}$$

Here $\mathrm{int}[\xi]$ rounds ξ to the nearest smaller integer. ε is a small correction (in this work 10^{-6}), which is smaller than the typical difference between two adjacent points in Equation 1. Such correction has no physical meaning, but enforces that if r_n^{tr} belongs to the continuous interval $\left(0,\, 1\frac{R}{N_R}\right]$ where 0 is excluded and R/N_R is included into the interval, then the corresponding α_n is set to 1 through Equation 6; if $r_n^{\mathrm{tr}} \in \left(1\frac{R}{N_R},\, 2\frac{R}{N_R}\right]$, then $\alpha_n = 2$, and so on until $r_n^{\mathrm{tr}} \in \left((N_R - 1)\frac{R}{N_R},\, N_R\frac{R}{N_R}\right)$, which implies $\alpha_n = N_R$. The construction of the β_n is performed similarly.

The field $\vec{u}_{\alpha\beta}$ is constructed as follows: for every couple $(\alpha^*,\, \beta^*)$ inside the domain, the values of the radial, tangential and axial components of $\vec{u}_{\alpha^*\beta^*}$ are evaluated by averaging over all the respective components of $\vec{u}_n^{\mathrm{tr}}$ such that $\alpha_n = \alpha^*$ and $\beta_n = \beta^*$. If there are no such $(\alpha_n,\, \beta_n)$, then the values of the components of $\vec{u}_{\alpha^*\beta^*}$ are left undefined. This can be done in a computationally efficient way by initializing all the $\vec{u}_{\alpha\beta}$ and a matrix of integer counters $C_{\alpha\beta}$ to zero, cycle over the n and, inside the cycle, add the value of $\vec{u}_n^{\mathrm{tr}}$ to the corresponding $\vec{u}_{\alpha^*\beta^*}$ and increase $C_{\alpha^*\beta^*}$ by one. After the cycle ends, the components of every $\vec{u}_{\alpha^*\beta^*}$ are divided by its corresponding $C_{\alpha^*\beta^*}$ if the latter is not zero, otherwise are set to *NaN* ("not-a-number") value. The local value of the angular velocity can be computed by dividing the tangential component of $\vec{u}_{\alpha\beta}$ by the corresponding radius.

The result of this procedure is a vector field $\vec{u}(r,\, y)$ (or better, its discretized version $\vec{u}_{\alpha\beta}$), defined in the domain $(0,\, R) \times (0,\, H)$. This field can be considered as representative of the

instantaneous velocity field, defined in any radial plane, at any given time *t* comprised between t_2 and t_{n-1}. Hence, any quantity calculated from $\vec{u}(r, y)$ (or better, $\vec{u}_{\alpha\beta}$) has to be similarly considered as evaluated at a given time *t* comprised between t_2 and t_{n-1}.

As an estimation of the measurement uncertainty, the standard error calculated from the adapted standard deviation was employed for the rectangles the tracer passed through at least three times. For the rectangles it passed through once, the maximum value for the standard error over the domain as described above was used.

2.3. Calculation of shear rate

The approach of Dapelo et al. (2015) was followed in this work. Assuming axial symmetry, the average shear rate can be written as:

$$|\dot{\gamma}(r, y)| = \left|\frac{\partial u_r}{\partial y} + \frac{\partial u_y}{\partial r}\right| \quad \text{Equation 8}$$

and the average over a volume domain comprised between two radii $r_a \equiv aR$ and $r_b \equiv bR$, $0 \leq a < b \leq 1$, as:

$$\langle\dot{\gamma}\rangle_a^b = \frac{\int_0^H dy \int_a^b drr|\dot{\gamma}(r,y)|}{\int_0^H dy \int_a^b drr} \quad \text{Equation 9}$$

Equation 9 can be discretized with a central differencing scheme as described above:

$$|\dot{\gamma}|_{\alpha\beta} \approx \left|\frac{u_{r,\alpha,\beta+1} - u_{r,\alpha,\beta-1}}{y_{\beta+1} - y_{\beta-1}} + \frac{u_{y,\alpha+1,\beta} - u_{y,\alpha-1,\beta}}{r_{\alpha+1} - r_{\alpha-1}}\right| \quad \text{Equation 10}$$

Equation 9 can then be approximated with the rectangle rule method. Let $\xi_{\alpha\beta}$ be 0 if the rectangle $(\alpha\ \beta)$ has never been occupied by a tracer particle; 1 elsewhere. Then we have:

$$\langle\dot{\gamma}\rangle_a^b \approx \frac{\sum_{\beta=0}^{N_y}\sum_{\alpha=a}^{b}\frac{x_{\alpha+1}-x_{\alpha-1}}{2}\frac{y_{\beta+1}-y_{\beta-1}}{2}r_\alpha\xi_{\alpha\beta}|\dot{\gamma}|_{\alpha\beta}}{\sum_{\beta=0}^{N_y}\sum_{\alpha=a}^{b}\frac{x_{\alpha+1}-x_{\alpha-1}}{2}\frac{y_{\beta+1}-y_{\beta-1}}{2}r_\alpha\xi_{\alpha\beta}} \quad \text{Equation 11}$$

3. Materials and Method

3.1. PEPT experimental method

The radioactive isotope ^{18}F was produced in a dilute water solution using the Birmingham MC40 cyclotron, and ion exchange particles of density approximately 1 g/cc were labelled with this isotope following the method of Fan et al. (2006). To ensure the long term survival of the particle in the solution, a thin lacquer coating was applied to seal the radioisotope onto the surface of the particle effectively and prevent loss of activity to the surrounding media (which could potentially introduce additional noise to the measurement).

The positron camera used is a Forte dual-headed gamma camera (Adac Laboratories) which consists of two heads on a motorised gantry which permits rotation about a horizontal axis and a separation of 250-800 mm between the detectors. Each head contains a single crystal of sodium iodide activated with thallium (NaI(TI)) scintillator, 500 x 400 mm^2 and 16 mm thick, coupled to an array of 55 photomultiplier tubes (49 76-mm tubes and 6 50-mm tubes).

Each photomultiplier is connected to a separate analogue-to-digital converter (ADC) and a single board computer in the head controls the 55 ADC channels. When scintillation occurs in the crystal, its centroid is determined via software allowing a spatial resolution of the camera for a point source of approximately 0.6 mm. The data are recorded event by event on a computer for subsequent processing. (Parker et al., 2002)

The lab-scale digesters were set up between the two detectors of the positron camera and a single radioactive tracer particle was introduced into the digester as it was mixed. The PEPT algorithm was used to determine the instantaneous location of the particle in three dimensions. The algorithm parameters were optimised and pertinent data calculated using the standard methods outlined by Leadbeater et al. (2012).

3.2. Lab-scale digesters

The mechanically-mixed digester consisted of a 200 mm diameter plastic cylinder, 240 mm high. It was equipped with a four blade impeller (flat blades of 30 mm length x 20 mm high x 7 mm thick) positioned 50 mm above the base of the reactor and four baffles (10 mm length x 7 mm thick) evenly spaced around the digester wall as shown in Figure 1a. The cylinder was filled to a height of 175 mm. The digester was operating at mixing speeds of 50 rpm, 100 rpm, 150 rpm and 200 rpm.

The gas-mixed apparatus was the same as that used in Dapelo et al. (2015) and consisted of a 200 mm diameter plexiglass cylinder, 200 mm high, attached to a base plate with a 1 mm diameter orifice for air injection as shown in Figure 1b. The air flow was generated by a small compressor and set to a flow rate of 5.30 ml/s by a flowmeter with valve. The cylinder was filled to a height of 130 mm.

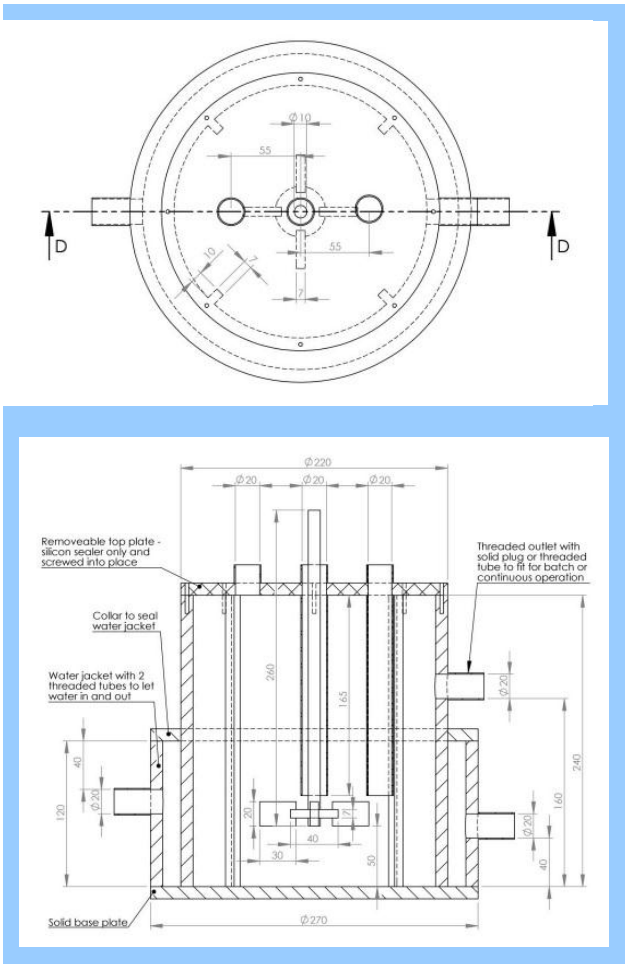

a)

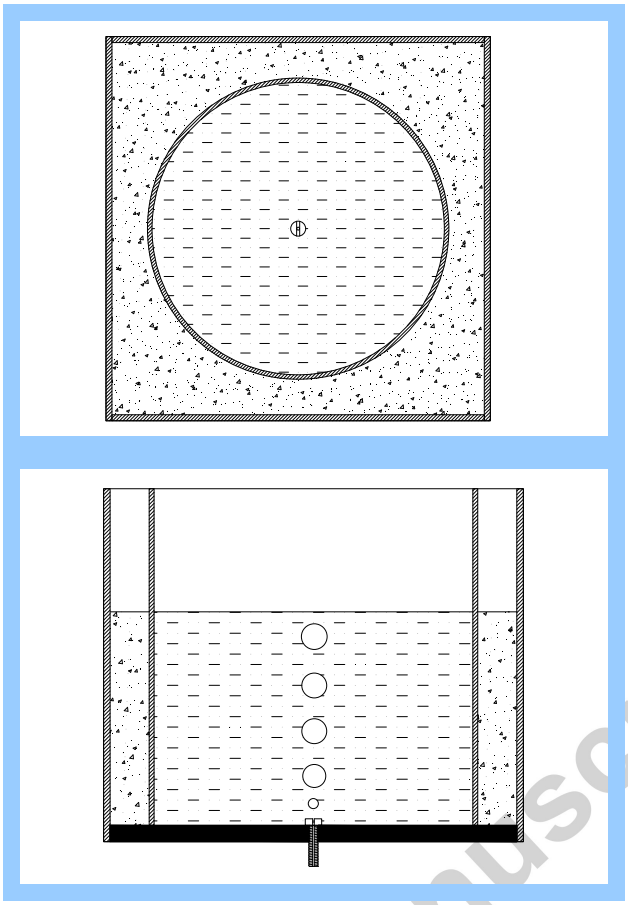

b)

Figure 1 - a) Design of mechanically-mixed digester, b) Design of gas-mixed digester, Dapelo et al (2015)

Two types of sludge were tested in the mechanically-mixed digester. The first sludge was anaerobically-digested sludge collected from the digesters at a local wastewater treatment works and is referred to here as 'real' sludge. The visualisation of mixing patterns present in an anaerobic digester, using real sludge, rather than a transparent model fluid, is only possible due to the application of PEPT to visualise flow in an opaque fluid. The second sludge was an opaque synthetic sludge, based on that used in Carliell-Marquet (2000). 0.1 g/l of carboxymethyl cellulose (CMC) was added in order to generate the required rheological properties of the sludge.
Both sludges were considered as non-Newtonian fluids that follow a power law model, $\eta = k\gamma^n$. The consistency index, k, and power law index, n were determined using a Couette viscometer (Fann Model 35). The total solids content of the two sludges were determined using the procedure described in Standard Methods (2540 B and E) (Eaton et al., 2005).

4. Results

4.1. Viscous properties of sludge

The rheological properties of real sludge and the three synthetic sludges used in the PEPT experiments were tested and the results are shown in Table 1 and Table 2 for the mechanically-mixed and gas-mixed experiments respectively.

Table 1 - Comparison of viscous properties and total solids of real and synthetic sludges for impeller-mixed experiments

Fluid	Consistency index, *k*	Power law index, *n*	Viscosity, mPa.s	Total solids content, g/l
Real sludge	0.0036	0.073	16	17.99
Synthetic sludge	0.2556	0.555	4	15.14

Table 2 - Viscous properties of synthetic sludge for gas-mixed experiments

CMC concentration, g/l	Consistency index, *k*	Power law index, *n*
2	0.054	0.805
4	0.209	0.730

4.2. Mechanically-mixed digester

Figure 2 and Figure 3 show the time evolution of the x, y and z coordinates of the tracer over a 20 minute period in the lab-scale anaerobic digester mixing real (Figure 2) and synthetic (Figure 3) sludge at a range of mixing speeds (50 rpm, 100 rpm, 150 rpm, 200 rpm). At high mixing speeds (150 rpm and 200 rpm), there are continuous oscillations in the *x*, *y* and *z* co-ordinates of the tracked particle. The occasional periods during which the co-ordinates of the particle do not change significantly correspond well to the location of the baffles suggest that the particle can become constrained against a baffle for a number of seconds before it re-enters the bulk fluid flow. The short duration of these occurrences indicates that particles that enter potential recirculation zones behind the baffles do not remain trapped there indefinitely.

At 50 rpm, the occurrence of these periods of limited motion are more frequent and can last over 5 minutes. The co-ordinates of the particle during these periods of slow movement occur when the particle is close to the digester walls, or is located either below the impeller or above 100 mm from the base of the digester (40 mm above the centre line of the impeller). This suggests that the impeller has a reduced sphere of influence on the motion of the sludge at low mixing speeds.

At 100 rpm, the synthetic sludge behaves more like the higher mixing speeds, with continuous oscillations of the particle co-ordinates, whilst the particle in the real sludge behaves like the lower mixing speed. This result is attributed to the rheology of the two sludges, with the impeller transferring less momentum to the more viscous real sludge than to the less viscous synthetic sludge.

i) ii)

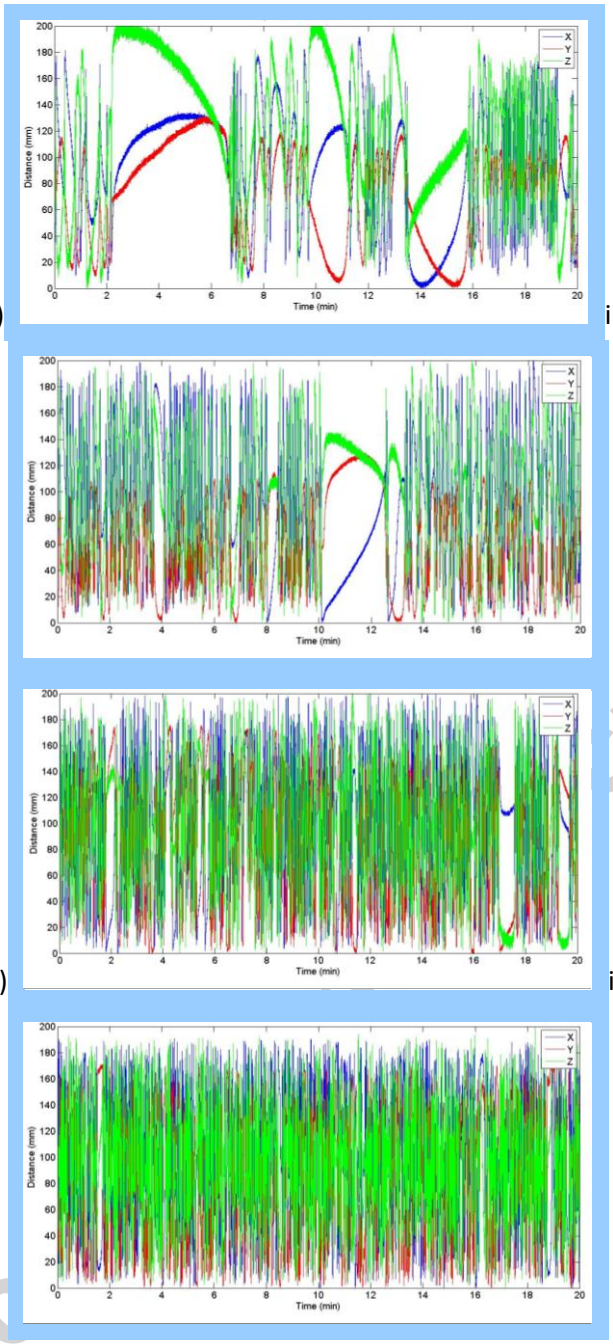

iii) iv)

Figure 2 – *x*, *y*, and *z* co-ordinates of a single radioactive particle over a 20 minute period in a lab-scale anaerobic digester mixing real sludge at i). 50 rpm, ii). 100 rpm, iii). 150 rpm, and iv). 200 rpm

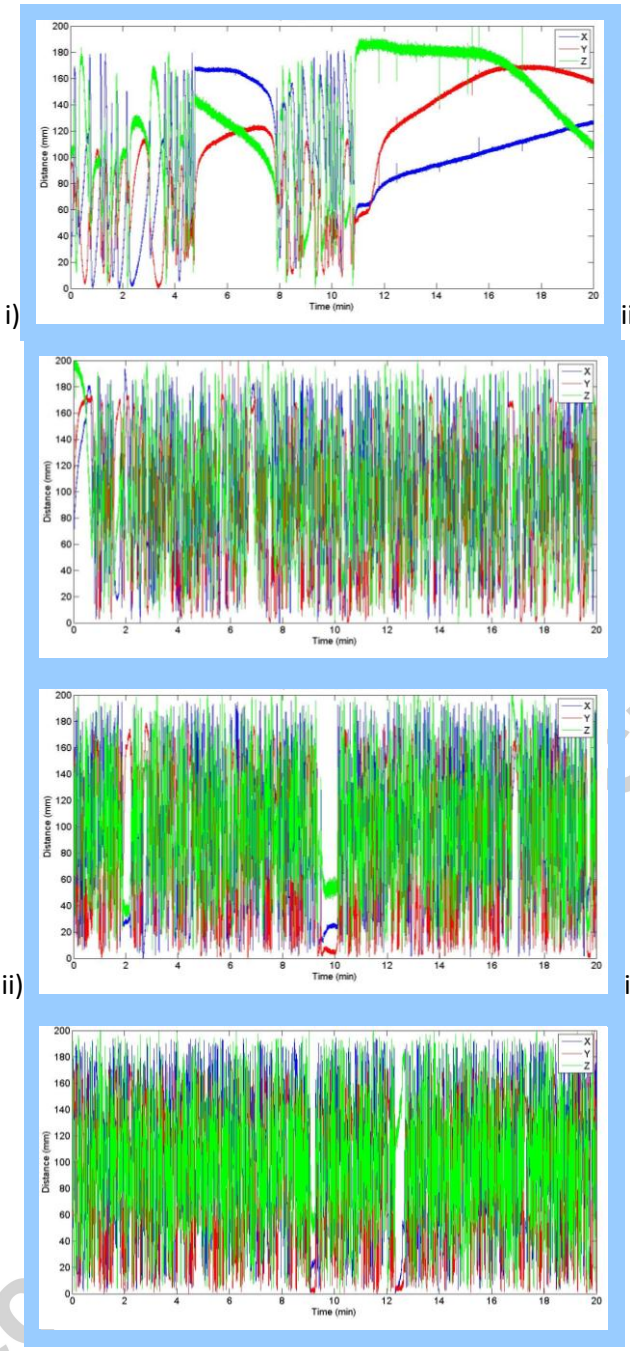

Figure 3 – *x*, *y*, and *z* co-ordinates of a single radioactive particle over a 20 minute period in a lab-scale anaerobic digester mixing synthetic sludge at i). 50 rpm, ii). 100 rpm, iii). 150 rpm, and iv). 200 rpm

The Cartesian co-ordinates of the particle at each point on its path were changed to cylindrical co-ordinates in order to calculate azimuthally-averaged variables. Azimuthal averages are commonly used in literature relating to stirred vessels, due to the axial symmetry of a cylindrical vessel. Once in cylindrical co-ordinates, a vertical two-dimensional grid was imposed on the digester between the axis of rotation (along the impeller shaft) and the wall of the digester. Each square in the two-dimensional grid represents all locations that fall within a three-dimensional toroidal cell, as shown in Figure 4.

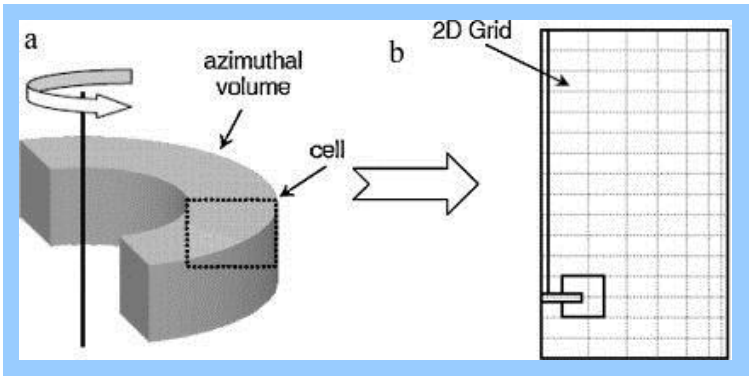

Figure 4 - Production of an azimuthal grid scheme for spatial averaging of data, taken from Chiti et al., 2011

Figure 5 and Figure 6 show the azimuthally-averaged occupancy of the digester taken as the time the particle spends in each grid cell as a percentage of the total time. As such, the sum of all grid cells add to 100 %, i.e. duration of particle monitoring. Establishing such occupancy plots for opaque sludge in a digester offers a valuable validation method for CFD models. As the cells used in this work are of the size width and height, the volume they represent varies across the width of the digester with the cells at the digester wall having a volume 100 times greater than those at the digester centreline. If the particle visited all parts of the digester equally this would result in a linear transition from occupancies of $1x10^{-5}$ % in cells at the centreline of the digester to $1x10^{-3}$ % in cells at the outer wall of the digester. Figure 5 and Figure 6 show that the occupancy of the cells is far from equal, even taking into account this discrepancy in cell volumes with maximum cell occupancies of 0.1 %, two orders of magnitude higher than the expected maximum when occupancy is evenly distributed. It can be seen that at 200 rpm, the occupancy is well-distributed across the digester, although it is higher in the outer regions of the digester, close to the walls, than it is around the impeller and impeller shaft at the centre of the vessel. This can be explained by the discrepancy in cell volumes and the fact that the flat-blade impeller acts as a radial flow impeller, pushing the fluid towards the walls of the digester before it moves around one of two circulation loops, above and below the impeller. Additionally, due to the speed at which the particle moves in regions close to the impeller and the smaller size of the cells, it is less frequently detected in this region, making it more difficult to accurately predict its location.

At 150 rpm, a very similar pattern to the occupancy plots at 200rpm is seen, although the existence of a zone of high occupancy at the base of the digester can be seen. This correlates with the particle's entry into a dead zone in Figure 2iii and 3iii. For real sludge at 100 rpm, the particle does not reach all parts of the digester, which explains the lack of data above 120 mm from the base of the digester and suggests that only some parts of the digester are effectively mixed. On the occasions when the particle does move through this upper third of the digester, it is moving slowly and so spends a great deal of time in these cells. This is seen again for both the synthetic sludge and real sludge at the lowest mixing speed of 50 rpm.

For real sludge at 50 rpm, there is an additional gap in the data, level with the impeller blades, where the tracer particle has not been recorded in the 20 minute period. It is likely that the run was too short for the particle to spend a significant enough amount of time in

the area for detection, especially given that these measurements were carried out when the particle was at its lowest activity. As the particle moves at a lower velocity, compared to at higher mixing speeds, the particle makes fewer "circuits" of the digester in the same amount of time. This low level of data capture close to the impeller, where the particle is moving at high velocity and is likely to be experiencing rapid changes in direction and velocity magnitude is a limitation of the PEPT technique, and has previously been noted by Chiti et al., 2011.

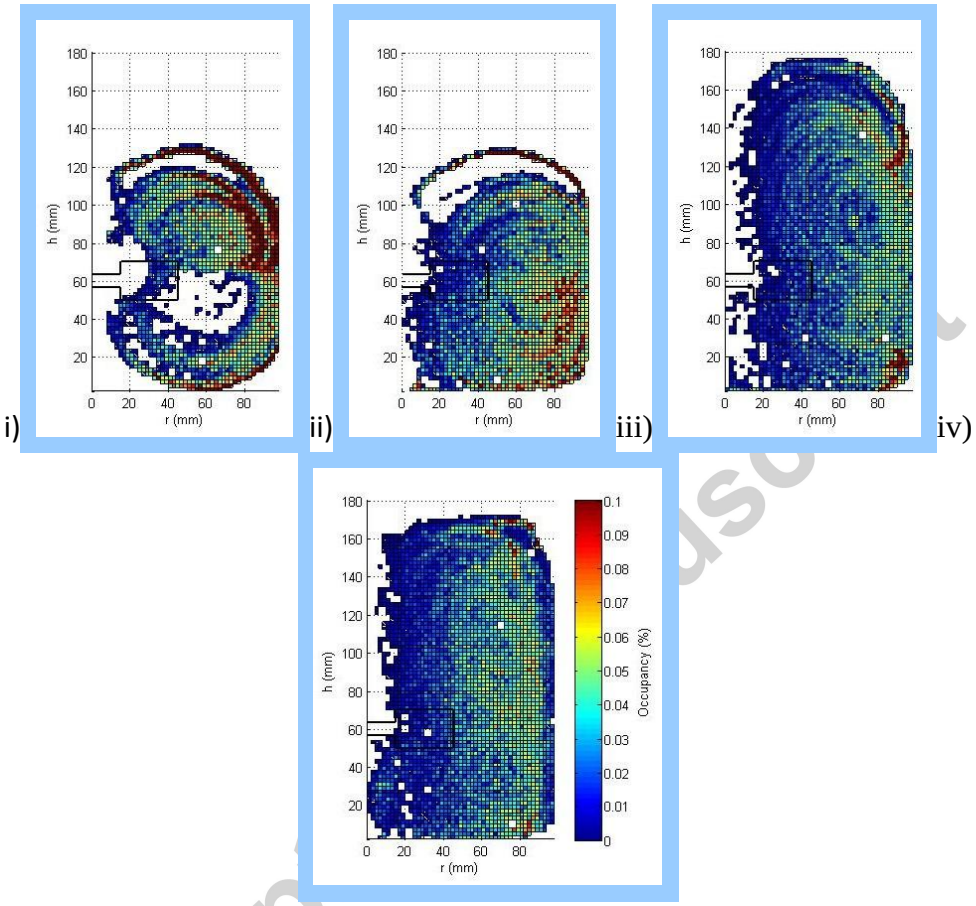

Figure 5 – Azimuthally-averaged occupancy in a lab-scale anaerobic digester mixing real sludge at i). 50 rpm, ii). 100 rpm, iii). 150 rpm, and iv). 200 rpm

i)

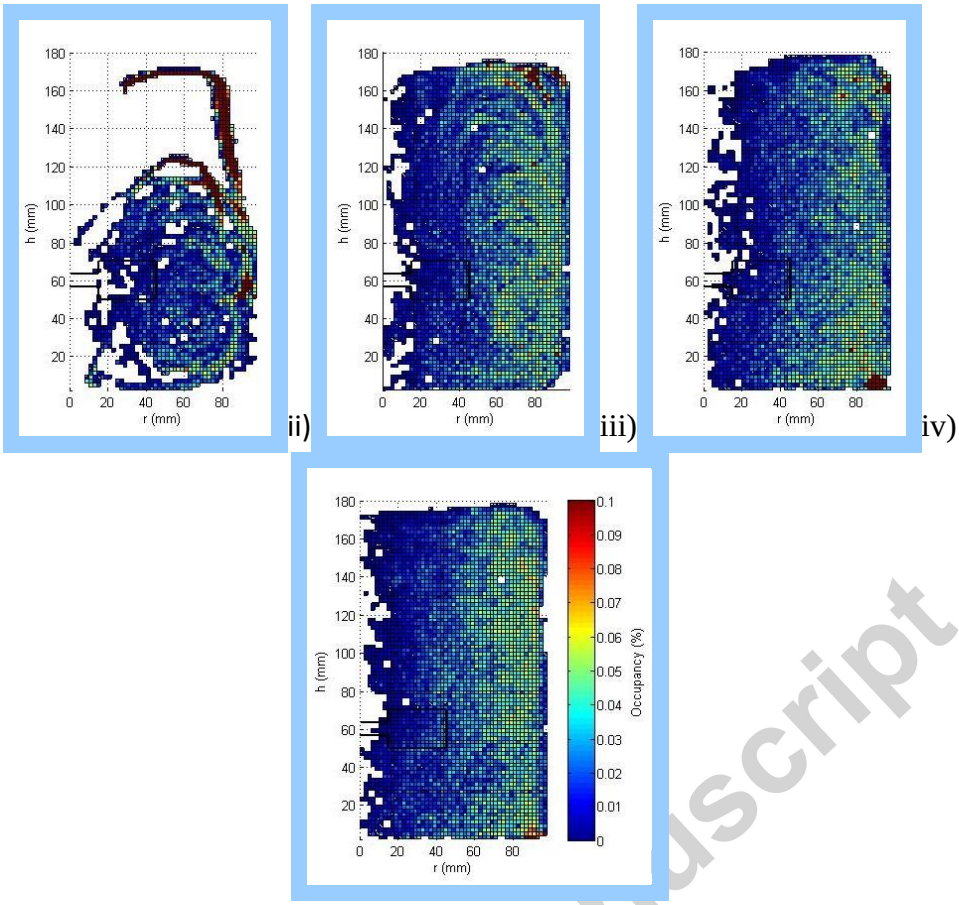

Figure 6 – Azimuthally-averaged occupancy in a lab-scale anaerobic digester mixing synthetic sludge at i). 50 rpm, ii). 100 rpm, iii). 150 rpm, and iv). 200 rpm

The velocity magnitude, axial and radial velocities are plotted as azimuthally-averaged variables, normalised by tip speed in Figure 7 to Figure 12.

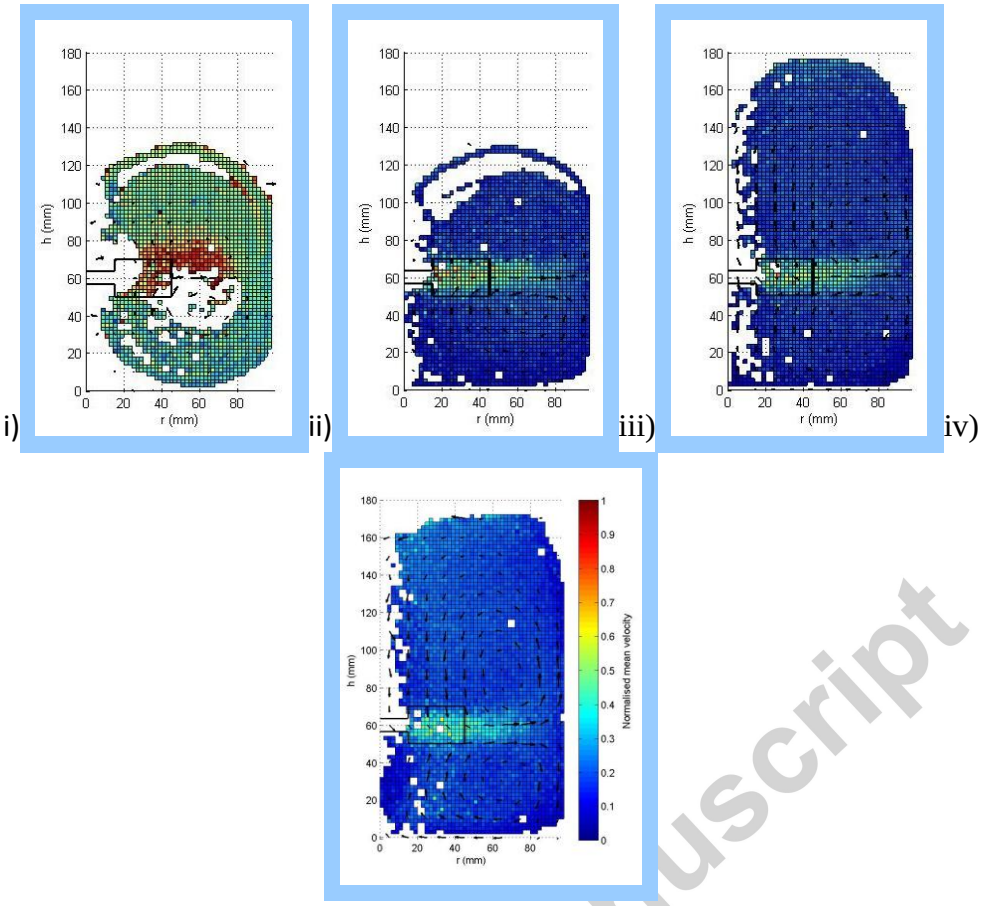

Figure 7 – Azimuthally-averaged velocity magnitude and velocity vectors, normalised by tip speed, in a lab-scale anaerobic digester mixing real sludge at i). 50 rpm, ii). 100 rpm, iii). 150 rpm, and iv). 200 rpm

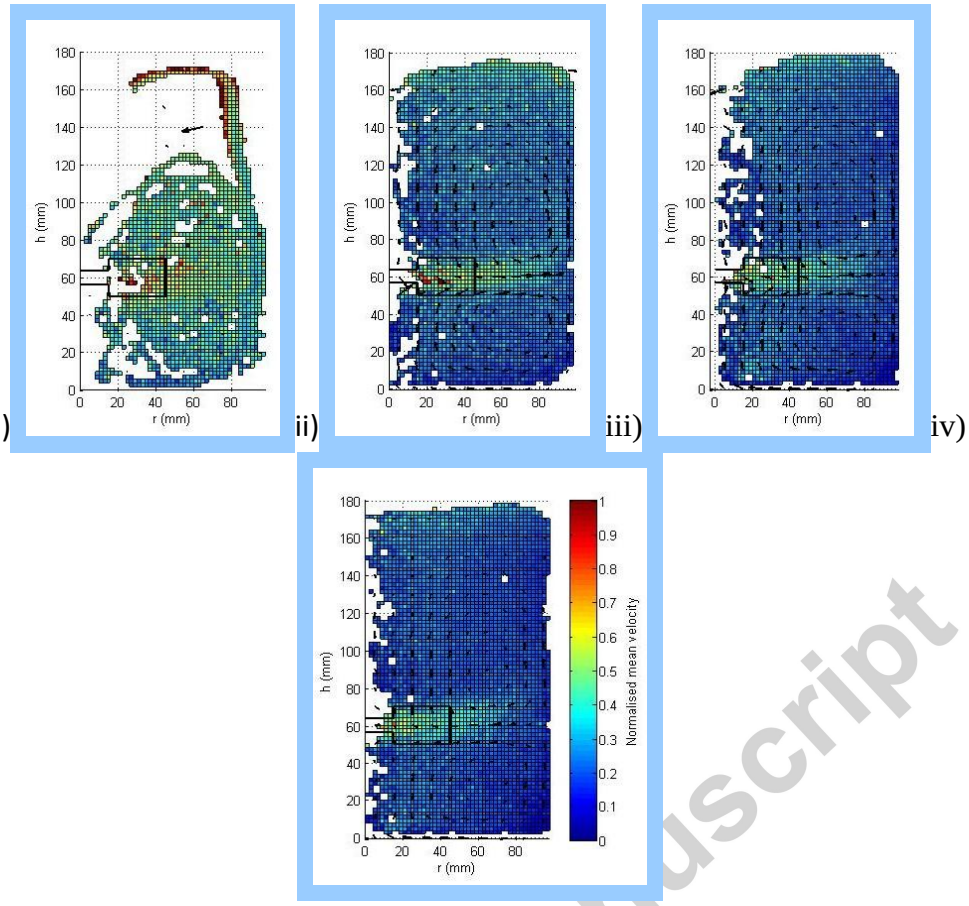

Figure 8 – Azimuthally-averaged velocity magnitude and velocity vectors, normalised by tip speed, in a lab-scale anaerobic digester mixing synthetic sludge at i). 50 rpm, ii). 100 rpm, iii). 150 rpm, and iv). 200 rpm

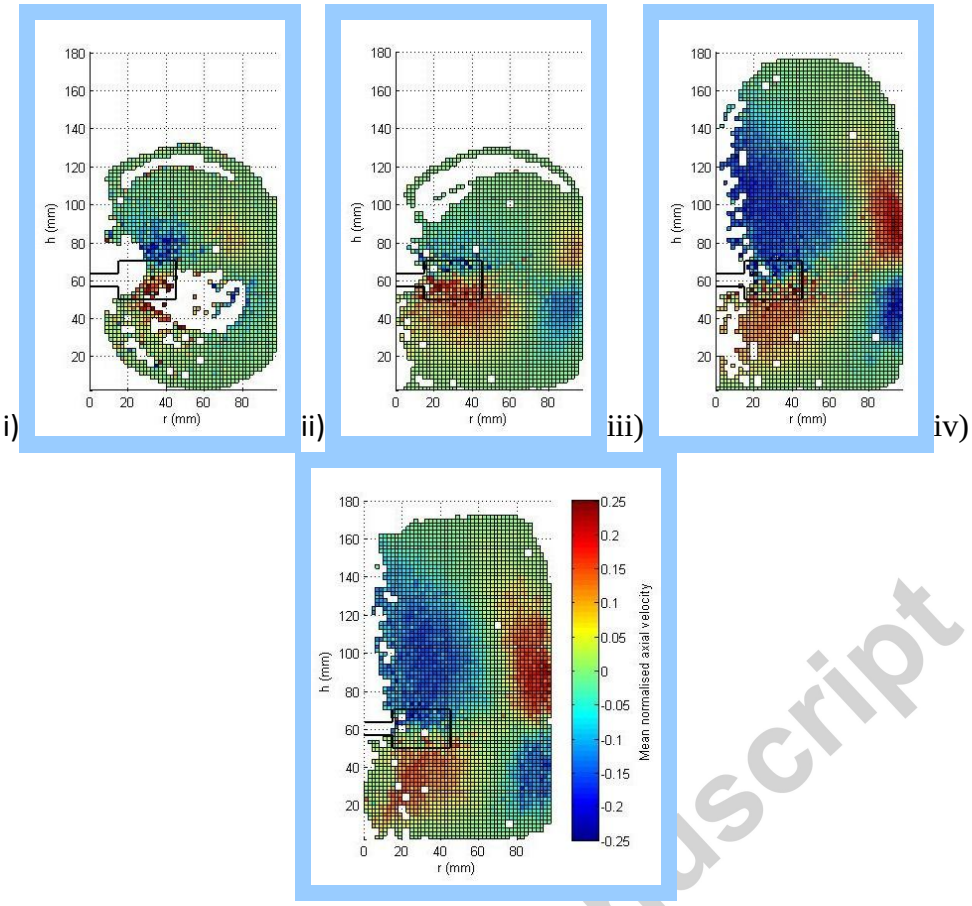

Figure 9 – Azimuthally-averaged axial velocity, normalised by tip speed, in a lab-scale anaerobic digester mixing real sludge at i). 50 rpm, ii). 100 rpm, iii). 150 rpm, and iv). 200 rpm

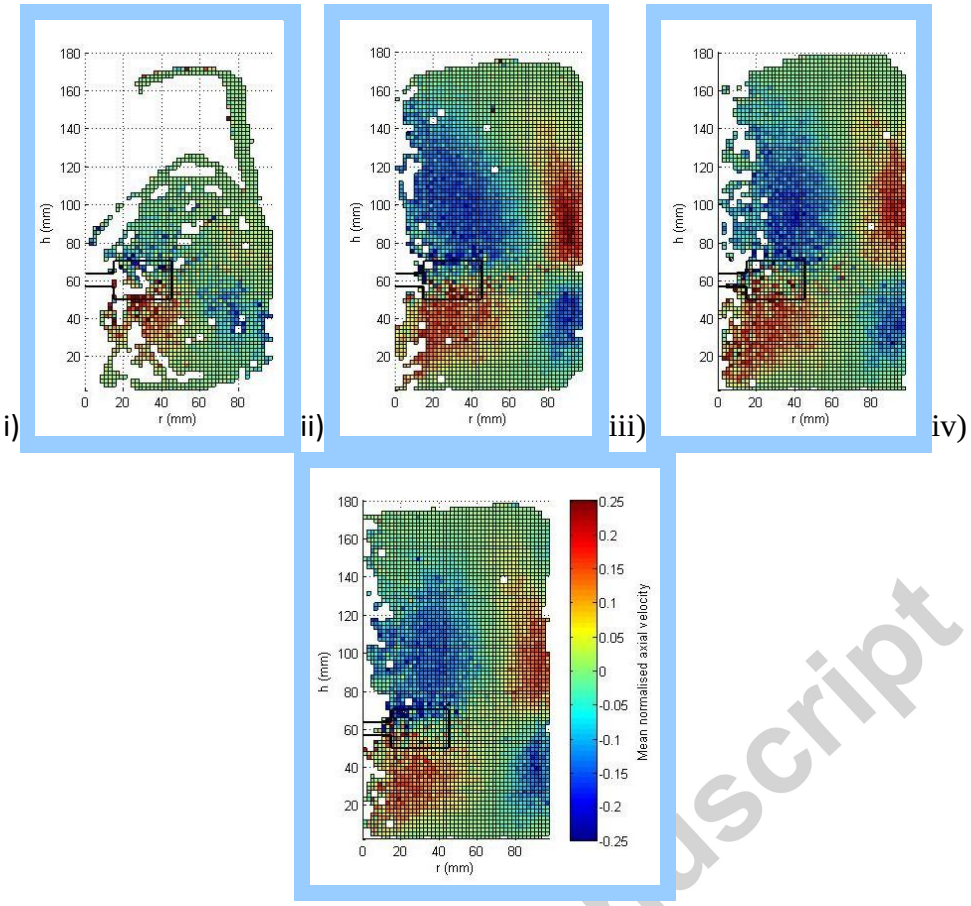

Figure 10 – Azimuthally-averaged axial velocity, normalised by tip speed, in a lab-scale anaerobic digester mixing synthetic sludge at i). 50 rpm, ii). 100 rpm, iii). 150 rpm, and iv). 200 rpm

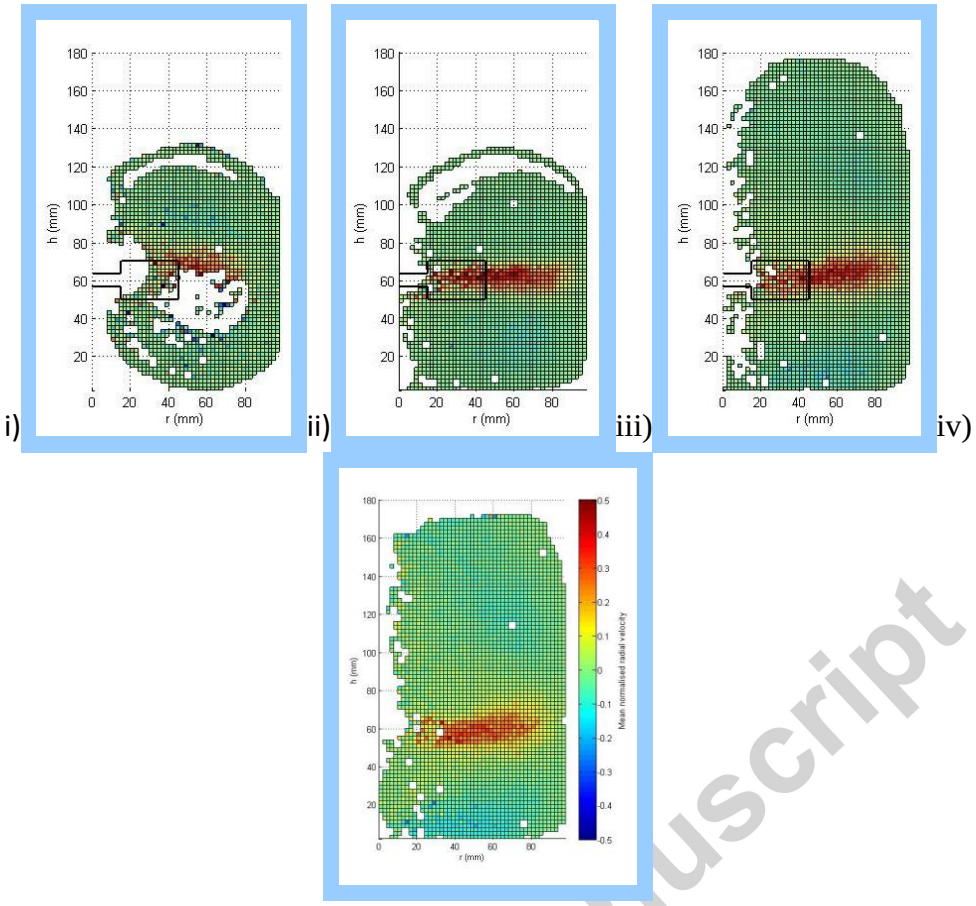

Figure 11 – Azimuthally-averaged radial velocity, normalised by tip speed, in a lab-scale anaerobic digester mixing real sludge at i). 50 rpm, ii). 100 rpm, iii). 150 rpm, and iv). 200 rpm

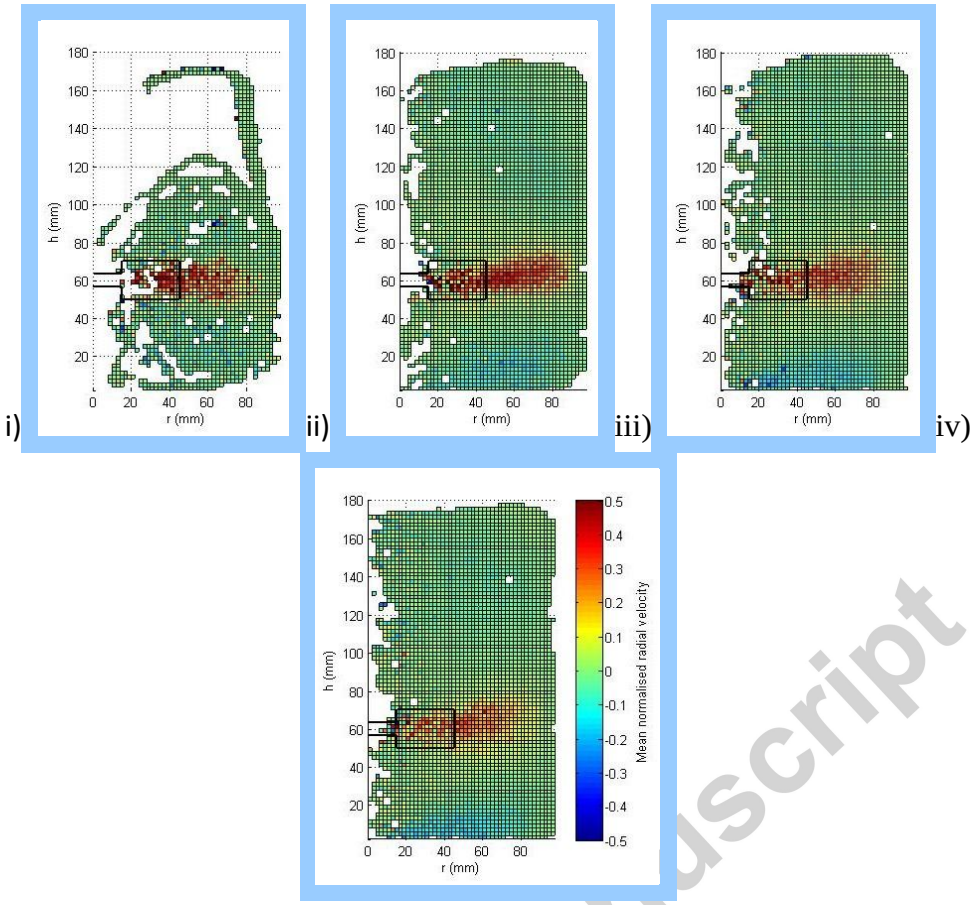

Figure 12 – Azimuthally-averaged radial velocity, normalised by tip speed, in a lab-scale anaerobic digester mixing synthetic sludge at i). 50 rpm, ii). 100 rpm, iii). 150 rpm, and iv). 200 rpm

Whilst the lack of data points recorded at 50 rpm make it more difficult to build up a detailed picture of the flow patterns in the digester, it can be seen that, once normalised by tip speed, the flow patterns in the digester for both real and synthetic sludge at all mixing speeds are similar. The mean normalised axial velocity plots demonstrate the upward flow of fluid along the wall of the digester above the impeller, and a reversal of flow direction back down towards the impeller, close to the shaft. Fluid velocity is higher close to the impeller region. Below the impeller, the mean axial velocity along the wall is negative as the fluid moves towards the base of the digester, with the return flow towards the impeller taking place close to the centre line of the digester. These two loops of fluid circulation are representative of a radial flow impeller and can be seen with little difference across the mean normalised axial velocity plots at all mixing speeds.

The mean normalised radial velocity plots demonstrate that the highest flow rate towards the wall of the digester takes place in line with the impeller. The rest of the digester experiences flow with little radial velocity, although a slight increase in negative radial velocity can be seen close to the base of the digester. This is more pronounced than the negative radial velocity in the recirculation loop above the impeller due to the limited space below the impeller.

4.2. Gas-mixed apparatus

One run was performed with the 2 g/l solution, and two with the 4 g/l solution. The tracer particle was expected to cover a shorter overall distance in the 4 g/l solution due to the higher viscosity, and consequently the 4 g/l runs were run for longer in order to have a comparable overall distance covered. Therefore, data were collected for approximately 30 minutes for the 2 g/l run, and 50 minutes for the 4 g/l runs. Care was taken to change the initial tracer position between the first and second run in the 4 g/l fluid. In particular, the tracer was dropped on the surface, in the middle of a quadrant. Two different quadrants were chosen as starting points for the two runs. The time evolution of the x, y and z coordinates of the tracer during each run are shown in Figures 13 a-b. The time evolution of the coordinates are correlated with one another in each run. They consist of a main oscillatory mode of about 0.1 Hz for the 2 g/l run, and between 0.1 (first run) and 0.01 Hz (second run) for the 4 g/l runs.

The main oscillatory mode is modulated by modes of period comparable with the time span of the runs. The secondary modes have little effect on the 4 g/l runs; however, they create a chaotic pattern on the 2 g/l run. The phase angle appears to be constant through the small cyclic oscillations, with abrupt changes during the rising of the tracer particle. This behaviour is more evident in the 4 g/l runs, where the phase remains approximately constant through the whole runs, with peaks at each particle rise. This suggests that changes in the phase angle have to be imputed to the conjunct effects of chaotic disturbance occurring when the tracer particle impacts the bubble column at the centre of the tank, and oscillations surviving the filtering process. Away from the limited zone enclosing the bubble column, the fluid motion can be considered as essentially planar, and thus angular velocity and tangential velocity components were considered as negligible.

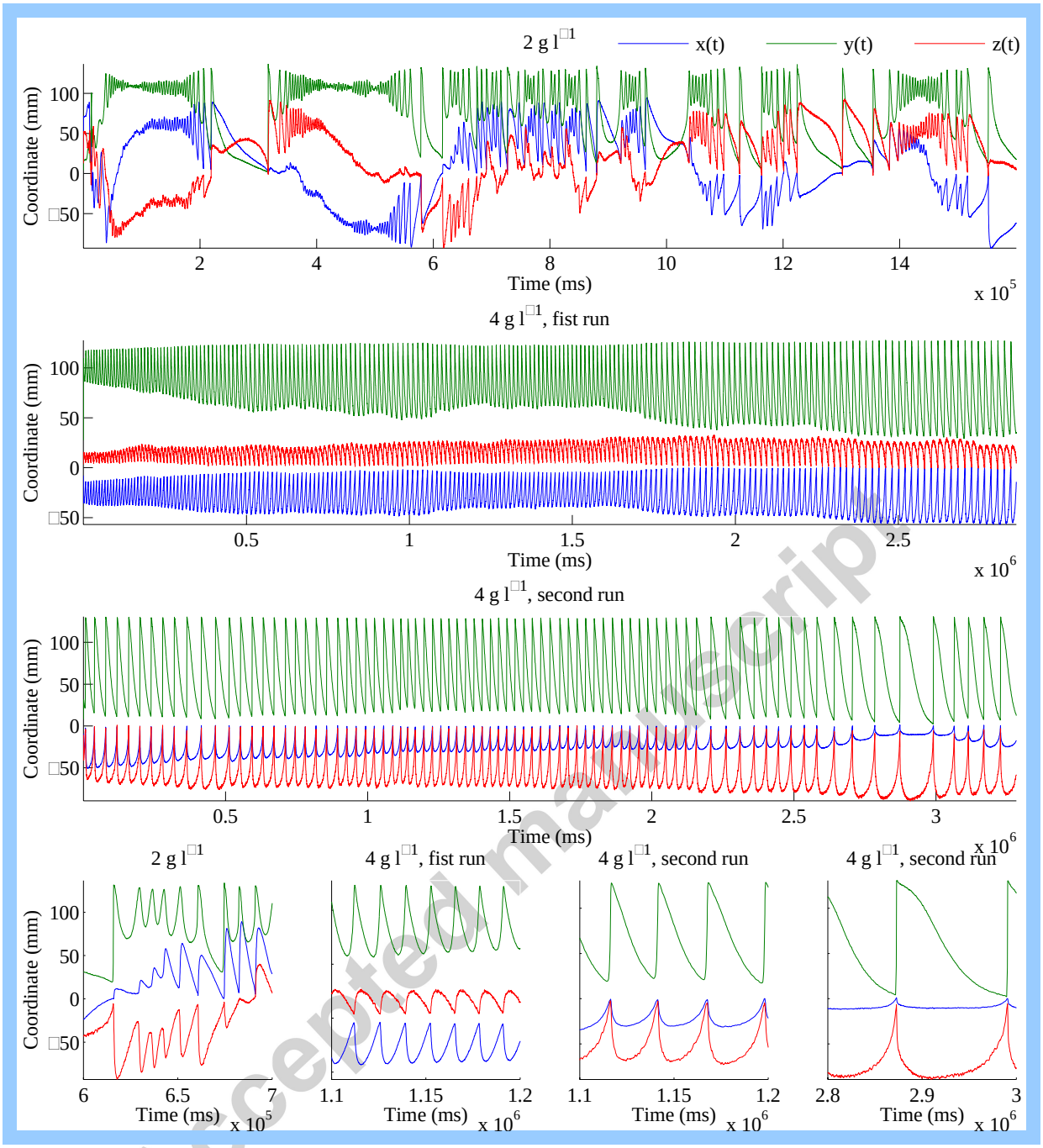

Figure 13a – Time evolution of the tracer position during the gas-mixed PEPT runs: Cartesian coordinates

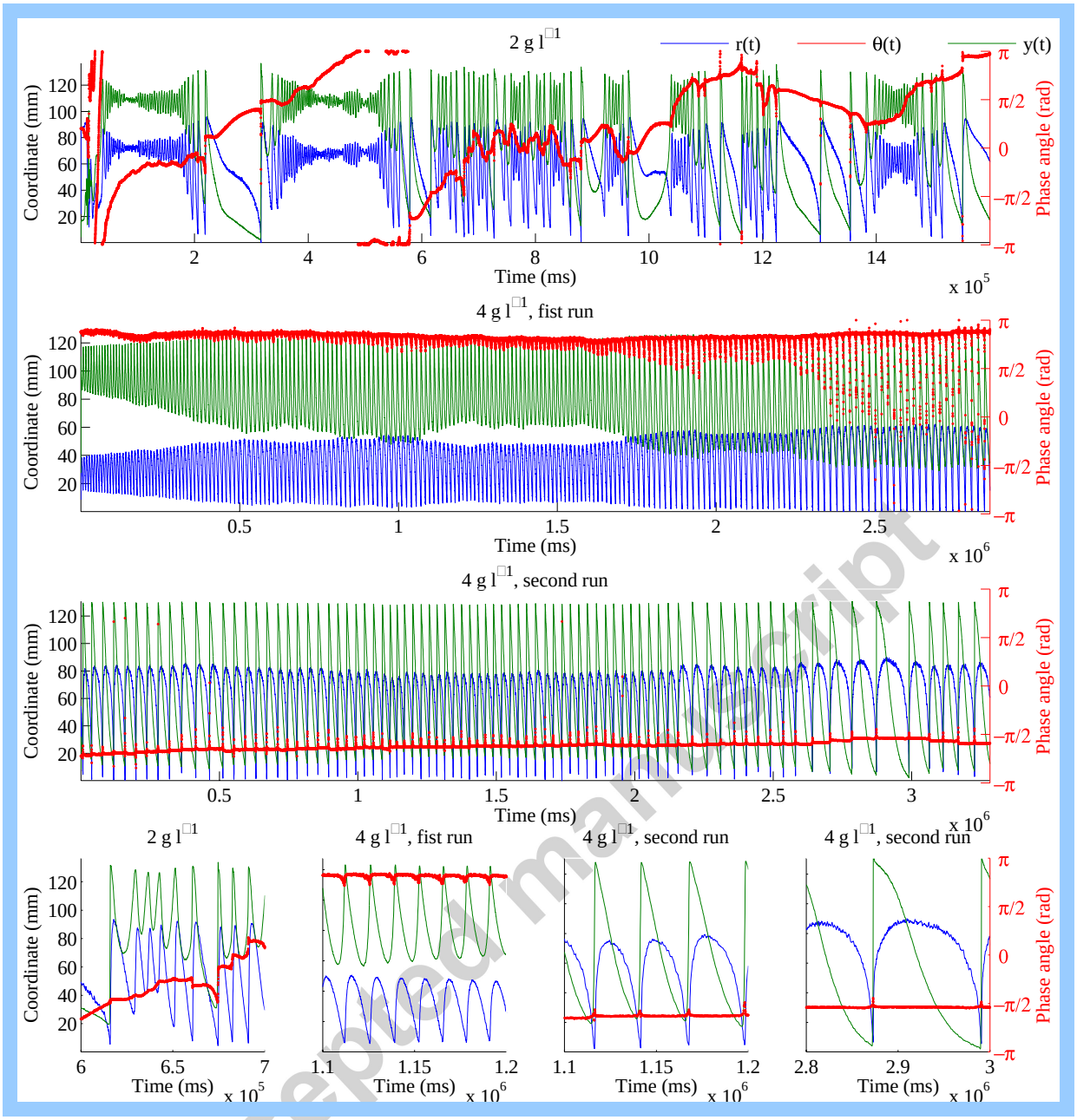

Figure 13b – Time evolution of the tracer position during the gas-mixed PEPT runs: Cylindrical coordinates

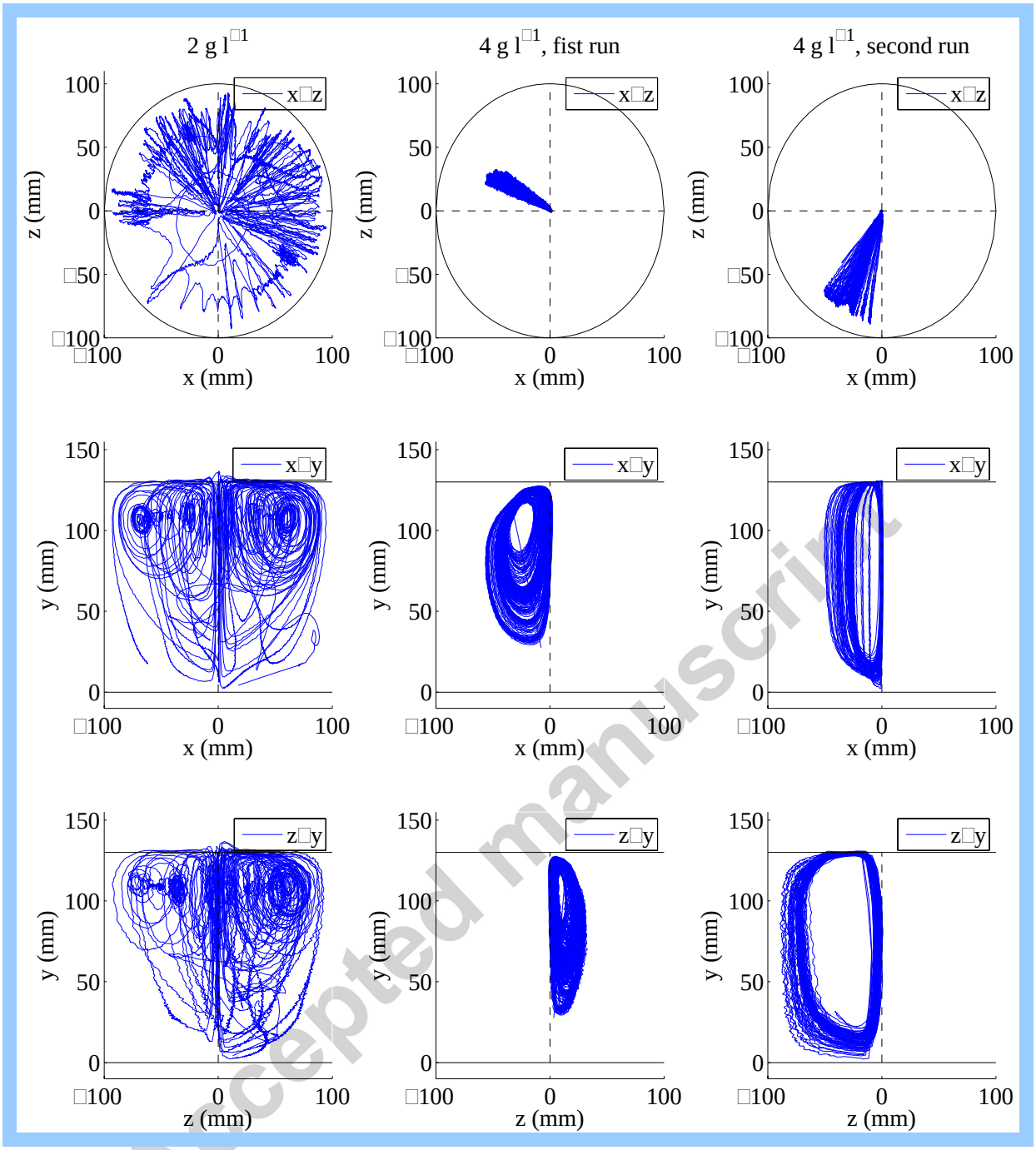

Figure 14 – Trajectory of the tracer. Projections over the x-z, x-y and y-z planes.

The trajectories of the tracer are shown in Figure 14. In each run, the tracer can be seen to follow a quasi-cyclical trajectory in which the particle is first swiftly dragged upwards by the central bubble plume, and then revolves around a toroidal vortex approximately 100 mm above the bottom of the tank. The trajectory lies onto a radial plane, and the radial symmetry of the flow is evident. The trajectory is not perfectly cyclical as a precession of the plane onto which it lies is clearly noticeable in every run. Additionally, the radius of the cycle varies considerably. While this occurs smoothly in the 4 g/l runs, frequent and abrupt changes can be noticed in the 2 g/l run. Those deviations from a perfectly cyclical trajectory can be interpreted as a disturbance due to the pulsating nature of the bubble column. In

fact, even though the air is injected at a constant flow rate, it arranges itself into discontinuous bubbles once inside the system, as shown in Figure 15. The momentum transfer from air to liquid is therefore pulsating, and this can force the tracer particle to change its cyclic radial-symmetric trajectory smoothly (as mainly seen in the 4 g/l runs) or abruptly (as seen in the 2 g/l runs), depending on the viscosity of the liquid phase.

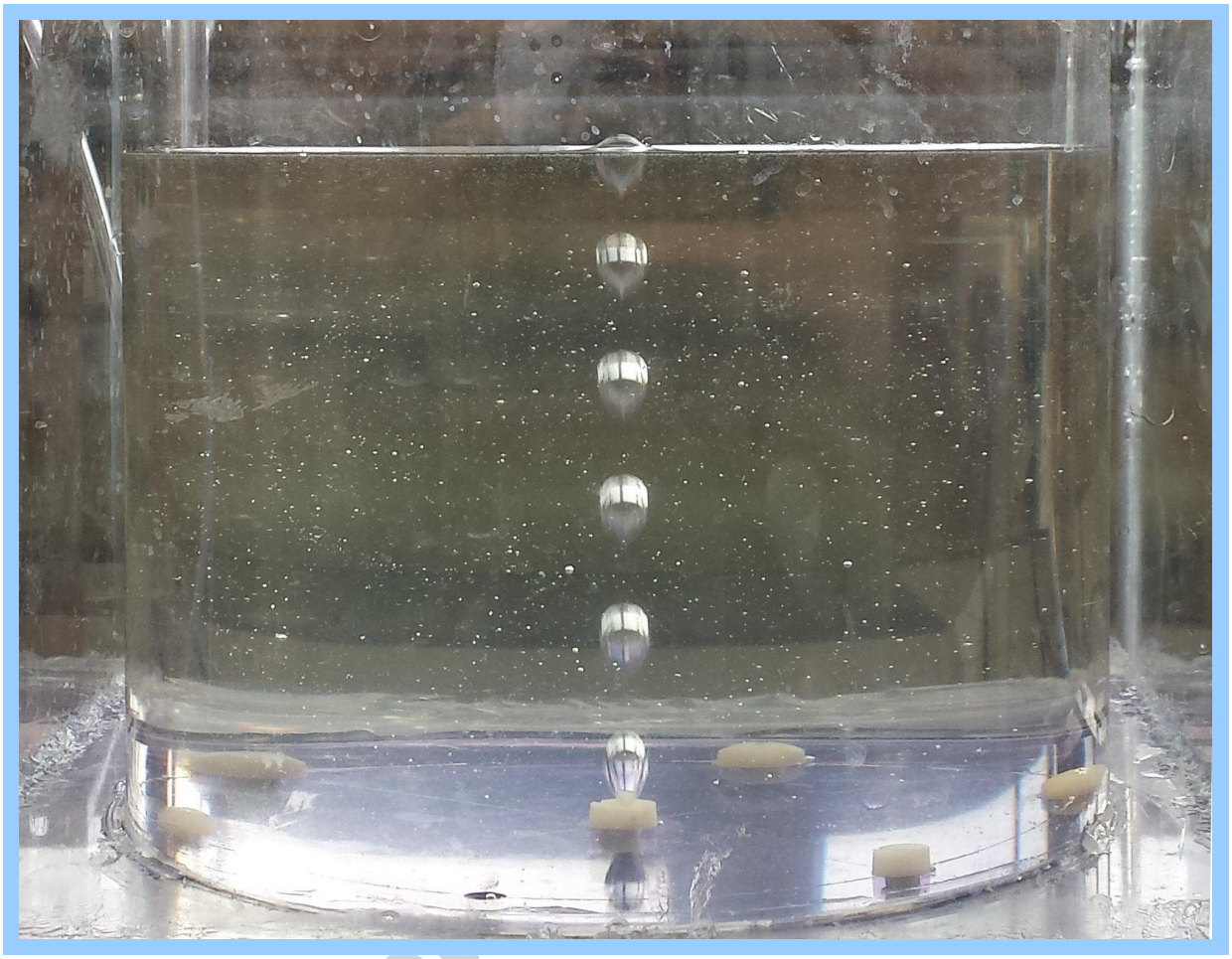

Figure 15 – Discontinuous bubble column

With the 4 g/l runs, it is noticeable that in each run the tracer spans a narrow zone of the domain – closer to the vortex in the first run, and closer to the sides of the vessel in the second run. This implies that the degree of mixing is poorer, and the trajectory strongly dependent on the initial conditions (starting location of the particle) in more viscous solutions. Figure 14 demonstrates that the trajectories lie in the same quadrants in which the tracer was released. The azimuthally-averaged occupancy is shown in Figure 16. Generating experimental occupancy plots for gas mixed digesters, offers a direct comparison to, and validation of, CFD models. In the 4 g/l solution, the particle becomes trapped into a circular path, as already displayed in Figure 14. With the 2 g/l solution, the particle spans a wider area, but spends about 60 % of the time at the centre of the toroidal vortex. A comparison with the time evolution in Figure 12 shows that the particle undergoes a sequence in which it first spans a large part of the domain, then becomes trapped inside the vortex and oscillates there for long time before escaping and repeating the sequence.

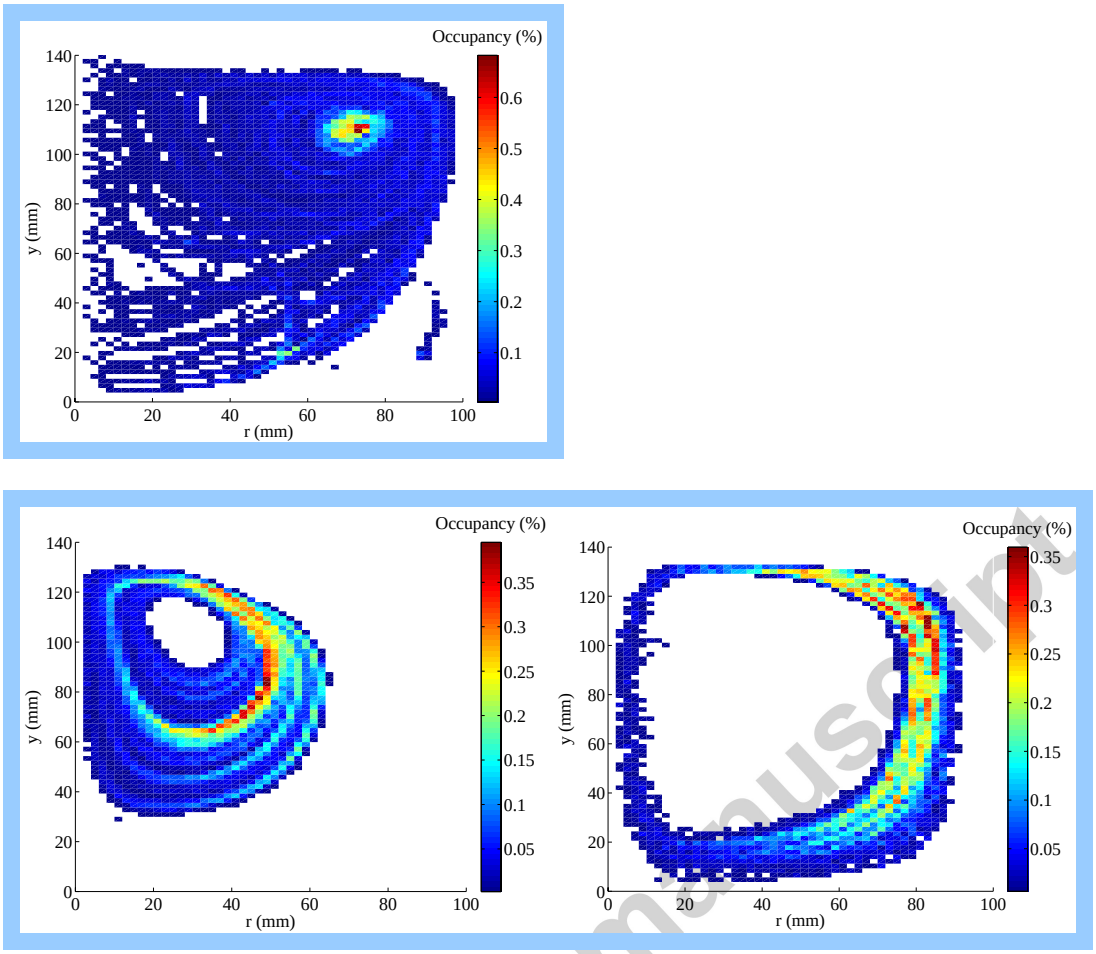

Figure 16 – Occupancy for the gas-mixed apparatus: 1) 2 g/l, 2) 4 g/l first run, 3) 4 g/l second run

The azimuthally-averaged mean velocity is shown in Figure 17. The two runs performed with the 4 g/l solution have been combined. The figure confirms the presence of the flow patterns identified in Dapelo et al. (2015) including the rapidly-rising column in proximity to the central bubble column, the horizontal displacement once the flow reaches the surface, the toroidal vortex and the velocity decrease in the lower part of the tank. For both solutions, the vortex can be identified as a relatively quiet zone surrounded by a circular crown in which the velocity is higher. In the 4 g/l solution, the particle was trapped in circular trajectories larger than the vortex, and so the vortex could not be tracked directly. However, the structure of the flow patterns in the surrounding area is qualitatively similar to that surrounding the vortex in the 2 g/l solution.

As the fluid viscosity increases, the central column is largely unaffected, but, the average velocity is reduced and the size of low velocity zones increase, especially near the walls of the vessel. In both cases, the vortex is formed by the downward movement of the rapidly moving liquid close to the surface. In the 2 g/l solution, the liquid moves downwards close to the vessel wall, while in the 4 g/l it does so at approximately r/3. Consequently, in the 4 g/l solution, the vortex is situated closer to the bubble column, and thus, the flow close to the vessel walls is reduced.

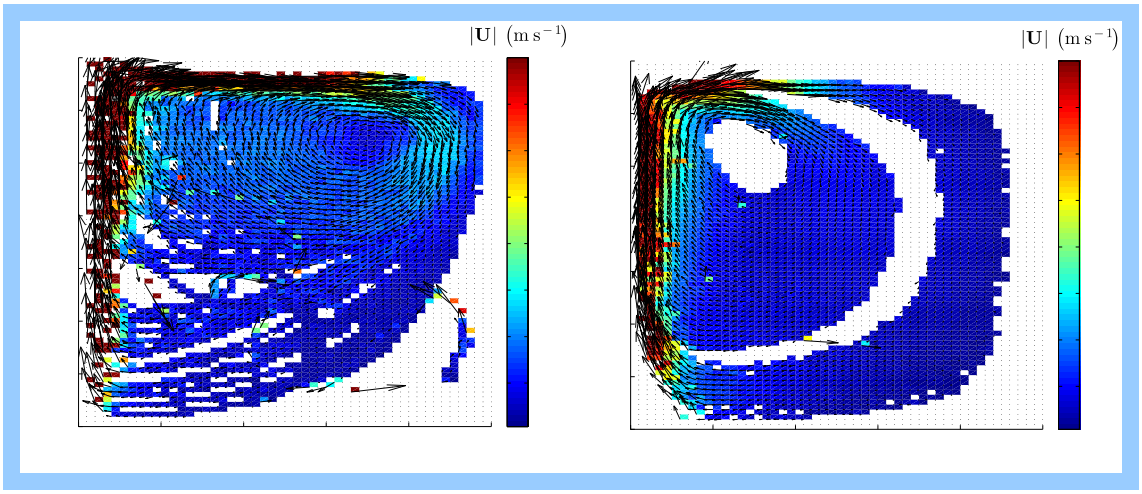

Figure 17 – Azimuthally-averaged velocity for the gas-mixed apparatus: Left: 2 g/l, Right: 4 g/l

4.3. Bubble column velocity and average shear rate in gas-mixed apparatus

The velocity profile shown in Figure 17 is similar to an analogous experiment conducted with the same experimental rig using PIV for flow field analysis (Dapelo et al., 2015). That work raised the issue of the accuracy of the PIV measurements at the bubble column. The laser beams originating from the central zone of the domain had to pass through the bubble column to reach the detector, and therefore experienced diffraction through the bubbles. Consequently, the CFD simulations described therein did not agree with the PIV data. As PEPT measurements are unaffected by the optical characteristics of a material, a comparison between PEPT, PIV and CFD simulations close to the bubble column is worthwhile.

Dapelo et al. (2015) validated their CFD model using average shear rate as a parameter. However, they pointed out that shear rate is expected to encompass several orders of magnitude due to the coexistence of turbulent and dead zones, and consequently, they proposed a subdivision of the domain into fixed zones of relatively homogeneous shear rate. Concentric domains were chosen to take advantage of axial symmetry in the vessel.

Four different domains were defined: (0, R), (0, 0.2 R), (0.2 R, 0.5 R) and (0.5 R, R). Figure 18 shows the average shear rate over these domains. In all cases, the simulated data better approach the PEPT data in the inner domains than in the outer domains. This was expected as the tracer passes through them more frequently.

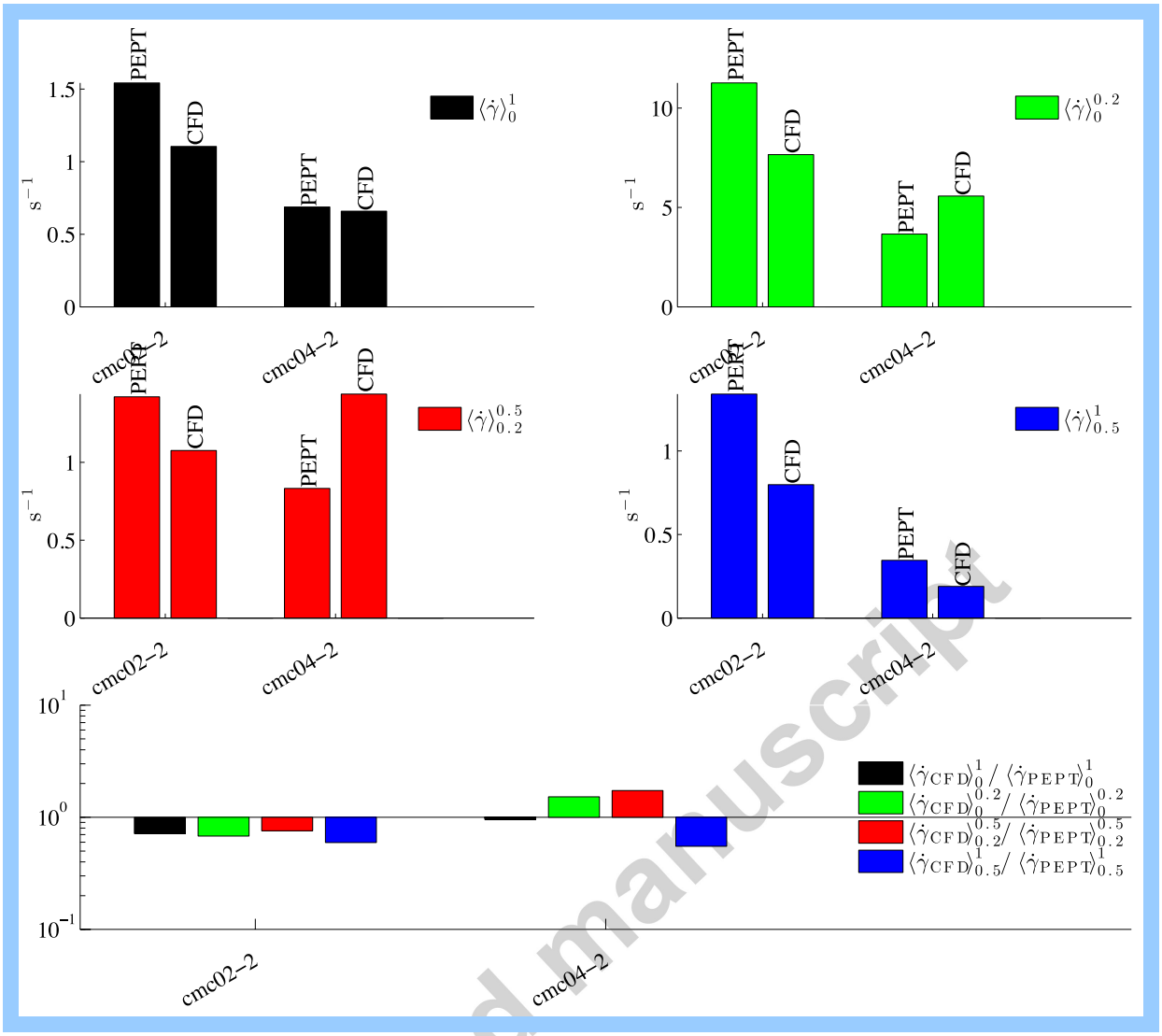

Figure 18: Average shear rate calculated over concentric subdomains: comparison between PEPT and CFD data from Dapelo et al. (2015).

A direct comparison between the PEPT measurements recorded here and the PIV and CFD data from Dapelo et al. (2015) is shown in Figure 21. It was not possible to trace comparisons in the region R<0.03 m because all the measurements reported in Dapelo et al. (2015) referred to a vertical plane placed at the distance of 0.03 m from the symmetry axis. Nevertheless, it is evident that the PIV data approach the CFD simulations in the outer region of the domain better than PEPT. This was expected, as the PEPT data in the outer regions are poor when compared with the inner parts of the digester, whilst for PIV this issue does not arise as the tracer microparticles diffuse uniformly through the liquid phase. Dapelo et al., 2015 failed to validate the CFD model in the inner part of the domain, near the bubble column, as discussed above, and the discrepancies between PIV and CFD data were of at least one order of magnitude. Conversely, PEPT is seen to be capable of giving robust measurements in the central part of the domain, and the data presented here show a much better agreement between CFD and PEPT data in the inner subdomains.

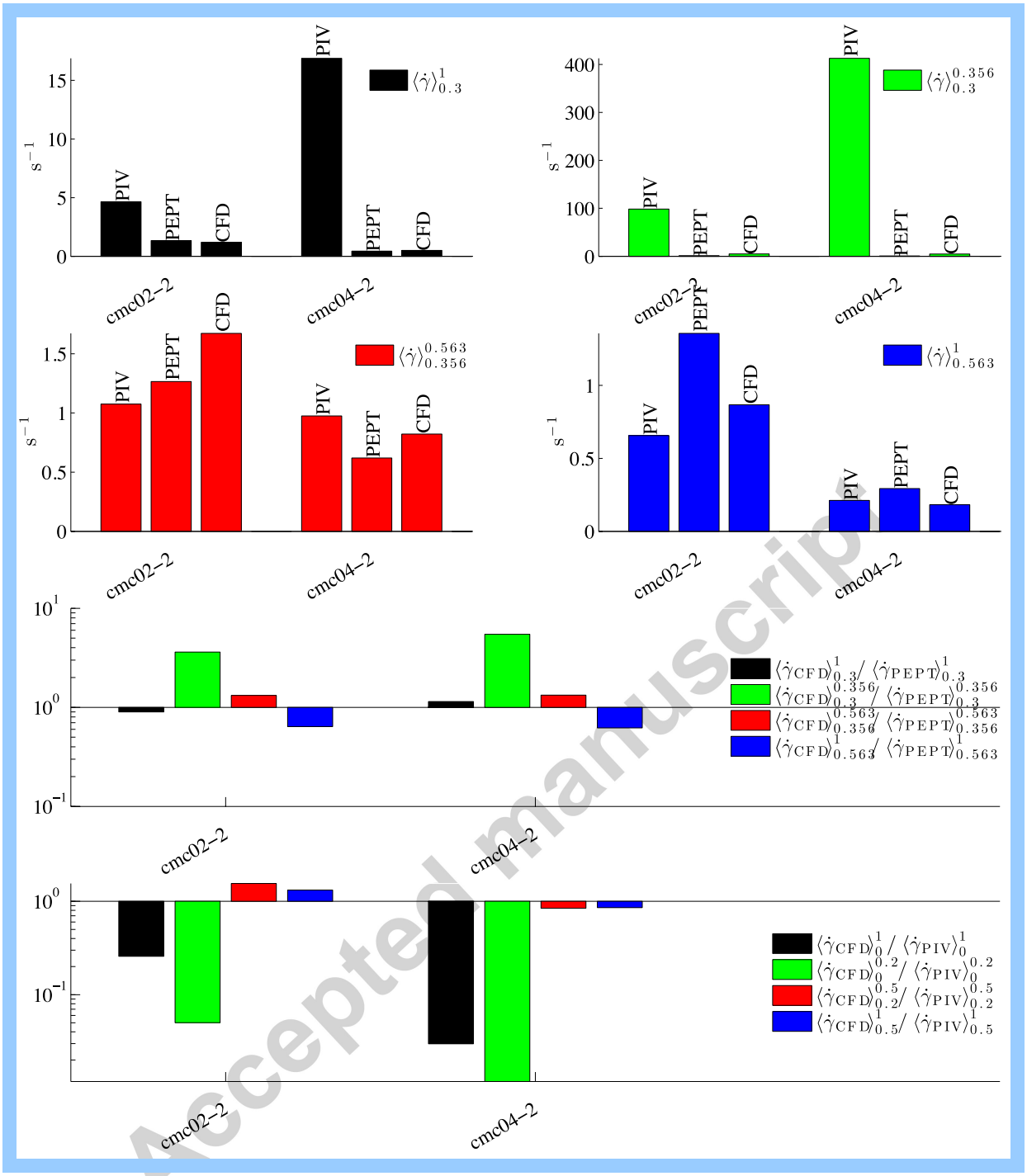

Figure 19: Average shear rate calculated over concentric subdomains: comparison between PEPT, PIV, and CFD data (from Dapelo et al. 2015).

5. Discussion

5.1. Differences between mechanical and gas mixing

The application of PEPT to lab-scale digesters has clearly demonstrated that mechanical and gas mixing mechanisms establish different flow patterns in the digester. Whilst both mixing methods establish a quasi-torodial flow path in the sludge, the location and spread of that flow path is heavily dependent on the mixing method and mixing speed. In the

mechanically-mixed digester, there are two fluid circulation loops, one above and one below the impeller whilst the bubble column in the gas-mixed digester gives rise to a single recirculation loop. It can be seen that low mechanical mixing speeds lead to poorer mixing than higher mechanical mixing speeds. The possible exception to this is in the area around the impeller blades, where the shear generated by the moving blades may ensure that the sludge is thoroughly mixed. This is suggested by the high speeds at which the particle appears to move through the area around the impeller blades compared to other areas of the digester when mixed at low speeds. However, the same high speeds lead to low data capture around the impeller blades and it is difficult to draw clear conclusions about the quality of mixing in this area of the digester.

5.2. Effect of sludge rheology

With both mixing mechanisms, the effect of sludge rheology is clear. Mixing is less successful with more viscous liquids, unless mixing power is increased to compensate for the increase in viscosity. This is clearly seen in the mechanically mixed digester at 100 rpm. The less viscous synthetic sludge is subjected to a higher degree of mixing, similar to that observed at higher mixing speeds. Meanwhile, the more viscous real sludge is subjected to a lower degree of mixing, similar to that observed at lower mixing speeds.

During the gas-mixing experiments using 4 g/l CMC solution, it is also noticeable that in each run the tracer spans a different zone of the domain—closer to the vortex in the first, and closer to the vessel walls in the second. This implies that the degree of mixing is poorer in more viscous solutions, and that the trajectory depends heavily on the starting point of the particle.

5.3. Benefits and limitations of PEPT

PEPT was used to visualise the flow patterns established by mechanical and gas mixing in lab-scale anaerobic digesters using opaque real sludge rather than a transparent synthetic sludge.

PEPT offers significant advantages over existing non-invasive flow visualisation techniques such as PIV and LDA. PEPT benefits from the ability to examine flow phenomena in three dimensions, as it is capable of tracking a particle as it moves around a three-dimensional volume. On the other hand, PIV is limited to recording data within the two-dimensional plane of the laser and LDA is only able to capture data at a single point. This greatly increases the ability of PEPT to construct a more complete picture of the flow patterns generated in a mixing vessel compared to more conventional flow visualisation techniques. This is a distinct advantage for flow visualisation in general, and for the validation of CFD models in particular. It is possible to carry out a direct comparison between PEPT data and CFD models to determine their ability to predict flow across a three-dimensional digester, rather than validating against a single point or a plane. For biogas production to be maximised by optimising flow patterns, it is valuable to be able to accurately validate a CFD model across the digester as a whole, as biogas production is unlikely to be uniform across a digester.

PEPT allows the examination of opaque fluids within opaque apparatus, which represents a critical advantage over traditional optical methods. Due to the inherent opacity of sludge, the visualisation of flow patterns within a digester cannot be carried out using conventional optical methods without the use of a synthetic fluid. This introduces an extra layer of complexity in choosing an appropriate transparent fluid with which to model the rheological properties of sludge (Eshtiaghi et al., 2012). From the results shown here, it is clear that rheology plays an important role in the degree of mixing achieved and consequently, the flow patterns that are established in an anaerobic digester. The rheological differences between the sludges tested here significantly alter the flow patterns established under the same mixing regime. Similar errors would be expected when attempting to recreate the properties of an opaque sludge in a transparent synthetic sludge. As such, removing the need for a transparent fluid makes the application of PEPT a desirable technique for flow visualisation in anaerobic digesters.

In the gas-mixed apparatus, it has been shown that PEPT is better able to capture flow patterns close to the bubble plume than PIV. PIV is limited in this region as the refraction and reflection of light by the bubbles distorts the reflection of light by the seeded particles, producing inaccuracies in the recorded location and hence the velocity of those particles. PEPT does not suffer from this limitation and shows good agreement with CFD models of the flow patterns in this region.

However, PEPT is not a flow visualisation technique without limitations. Chiti et al. (2011) compared PEPT results of mixing salt and sugar solutions with a Rushton impeller to LDA results and showed that, whilst generally the PEPT results compared well, they underestimated velocities in the impeller region. This was also noted in the current work, in particular in the impeller region, and was associated with low data capture due to the high velocity of the particle, and rapid changes in its direction and velocity magnitude. Similarly, the tracer particle rarely entered the areas of the gas-mixed apparatus furthest from the bubble column and it was observed that there was a substantial discrepancy between the PEPT results and the CFD simulations in those subdomains. Whilst this limitation will reduce the effectiveness of the technique in those regions, results may be improved by running the experiment for longer to collect more data.

6. Conclusions

The work reported in this paper considered the application of the non-invasive imaging technique, PEPT, to lab-scale anaerobic digesters. This facilitated a full analysis of the flow patterns that are generated by different mixing methods and speeds in opaque fluids. Both mechanical and gas-mixed digesters were tested at a range of mixing speeds and the differences between the flow patterns generated by impeller-driven and gas mixing were described. It was shown that higher mixing speeds are required to ensure the same level of mixing in a more viscous sludge, demonstrating the importance of selecting accurate rheological properties for sludge in order to generate the correct flow patterns. The challenge of recreating these properties in a transparent medium is removed when PEPT is used instead of other non-invasive flow visualisation techniques, as opaque fluids and vessels can be used.

The application of the PEPT technique allows validation of a CFD model in the central subdomain of a gas-mixed digester, where optical techniques such as PIV have previously proved unable to accurately visualise flow close to the bubble column. Furthermore, the ability to track flow patterns in three dimensions using PEPT allows CFD models to be validated across the entirety of the domain instead of validating against a single point or plane. This helps to ensure that CFD models of digesters are able to realistically reproduce flow patterns to optimise biogas production. Together with the possibility of producing measurements directly on opaque sludge, this advantage constitutes a decisive advance in the current drive to validate CFD models in lab-scale vessels in order to then apply them to full-scale designs.

Whilst PEPT is a valuable tool for flow visualisation within opaque fluids and vessels, there are limitations to the method. In particular, the area close to the impellers is associated with low data capture due to the high velocity and rapid changes of direction of the particle. Similarly, the measurements in the outermost regions of a gas-mixed vessel are affected by a bias originating from too few data points. It is believed that this could be overcome by extending the length of the experimental run.

Acknowledgements

The computational work reported in this paper was undertaken using the BlueBEAR High Performance Computing (HPC) facility at the University of Birmingham, UK. The authors are grateful for the use of this facility and the support provided by the University.

The first author was funded via an EPSRC CASE award in conjunction with Severn Trent Water. The second author was funded via a University of Birmingham Postgraduate Teaching Assistantship award.

References

Bakalis, S., Fryer, P.J., and Parker, D.J. (2004). Measuring velocity distributions of viscous fluids using positron emission particle tracking (PEPT). *AIChE Journal*, 50 (7), 1606-1613.

Bakalis, S., Cox, P.W., Russell, A.B., Parker, D.J., and Fryer, P.J. (2006). Development and use of positron emitting particle tracking (PEPT) for velocity measurements in viscous fluids in pilot scale equipment. *Chemical Engineering Science*, 61 (6), 1864-1877.

Barigou, M. (2004). Particle tracking in opaque mixing systems: An overview of the capabilities of PET and PEPT. *Chemical Engineering Research and Design*, 82 (9), 1258-1267.

Baudez, J.C., Slatter, P., Eshtiaghi, N. (2013). The rheological behaviour of anaerobic digested sludge. *Chemical Engineering Journal*, 215-216, 182-187.

Bridgeman, J (2012). Computational fluid dynamics modelling of sewage sludge mixing in an anaerobic digester. *Advances in Engineering Software*, 44.

Burton, C.H., and Turner, C. (2003). *Manure Management Treatment Strategies for Sustainable Agriculture* (2nd edn.). Bedford, UK: Silsoe Research Institute.

Carliell-Marquet, C. (2000). *The effect of phosphorus enrichment on fractionation of metals and phosphorus in anaerobically digested sludge*. PhD, University of Loughborough.

Chiti, F., Bakalis, S., Bujalski, W., Barigou, M., Eaglesham, A., and Nienow, A.W. (2011). Using positron emission particle tracking (PEPT) to study the turbulent flow in a baffled vessel agitated by a Rushton turbine: Improving data treatment and validation. *Chemical Engineering Research and Design*, 89 (10), 1947-1960.

Dapelo, D., Alberini, F., Bridgeman, J., 2015. Euler-Lagrange CFD modelling of unconfined gas mixing in anaerobic digestion. *Water Research*, 85, 497-511.

Dapelo, D., Bridgeman, J. 2015. Computational Fluid Dynamics Modelling of Unconfined Gas Mixing of Wastewater Sludge in a Full Scale Anaerobic Digester, in J. Kruis, Y. Tsompanakis, B.H.V. Topping, (Editors), *Proceedings of the Fifteenth International Conference on Civil, Structural and Environmental Engineering Computing*, Civil-Comp Press, Stirlingshire, UK, Paper 270. doi:10.4203/ccp.108.270

Eaton, A. D., Clesceri, L. S., Rice, E. W. & Greenburg, A. E. (eds.) (2005). *Standard Methods for the Examination of Water and Wastewater*, Washington D.C.: APHA-AWWA-WEF.

Fan, X., Parker, D., and Smith, M. (2006). Labelling a single particle for positron emission particle tracking using direct activation and ion exchange techniques. *Nuclear Instruments and Methods in Physics Research Section A: Accelerators, Spectrometers, Detectors and Associated Equipment*, 562 (1), 345–350.

Fangary, Y.S., Barigou, M., Seville, J.P.K., and Parker, D.J. (2000). Fluid trajectories in a stirred vessel of non-Newtonian liquid using positron emission particle tracking. *Chemical Engineering Science*, 55 (24), 5969-5979.

Hoffman, R., Garcia, M.L., Vesvikar, M., Karim, K., Al-Dahhan, M.H. and Angenent, L.T. (2008). Effect of shear on performance and microbial ecology of continuously stirred anaerobic digesters treating animal manure. *Biotechnology and Bioengineering*, 100, 38-48.

Holland, F.A., and Chapman, F.S. (1966). *Liquid Mixing and Processing in Stirred Tanks*, New York: Reinhold Publishing Corporation.

Leadbeater, T., Parker, D., and Gargiuli, J. (2012). Positron imaging systems for studying particulate, granular and multiphase flows. *Particuology*, 10 (2), 146–153.

Owen, W.F. (1982). Anaerobic Treatment Processes. *Energy in Wastewater Treatment.* Englewood Cliffs, NJ: Prentice-Hill Inc.

Parker, D.J., Broadbent, C.J., Fowles, C., Hawkesworth, M.R., and McNeil, P. (1993). Positron emission particle tracking – a technique for studying flow within engineering equipment. *Nuclear Instruments and Methods in Physics Research Section A: Accelerators, Spectrometers, Detectors and Associated Equipment*, 326 (3), 592-607.

Parker, D., Forster, R., Fowles, P., and Takhar, P. (2002). Positron emission particle tracking using the new Birmingham positron camera. *Nuclear Instruments and Methods in Physics Research Section A: Accelerators, Spectrometers, Detectors and Associated Equipment*, 477 (1-3), 540–545.

Perez-Mohedano, R., Letzelter, N., Amador, C., VanderRoest, C.T., and Bakalis, S. (2015). Positron emission particle tracking (PEPT) for the analysis of water motion in a domestic dishwasher. *Chemical Engineering Journal*, 259, 724-736.

Pianko-Oprych, P., Niewow, A.W., and Barigou, M. (2009). Positron emission particle tracking (PEPT) compared to particle image velocimetry (PIV) for studying the flow generated by a pitched-blade turbine in single phase and multi phase systems. *Chemical Engineering Science*, 64 (23), 4955-4968.

Sindall, R., Bridgeman, J, and Carliell-Marquet, C. (2013). Velocity gradient as a tool to characterise the link between mixing and biogas production in anaerobic waste digesters. *Water Science and Technology*, 67, 2800-2806.

Ward, A.J., Hobbs, P.J., Holliman, P.J., and Jones, D.L. (2008). Optimisation of the anaerobic digestion of agricultural resources. *Bioresource Technology*, 99 (17), 7928-7940.

Wu, B (2010). CFD simulation of gas and non-Newtonian fluid two-phase flow in an anaerobic digester. *Water Research*, 44, 3861-3874.

Wu, B (2012). Large eddy simulation of mechanical mixing in anaerobic digesters. *Biotechnology and Bioengineering*, 109.

Highlights

- PEPT was used for flow visualisation of mixing in lab-scale anaerobic digesters
- PEPT offered improved validation for 3D CFD models of mixing in anaerobic digestion
- PEPT was successful in opaque sludge, removing the need for mimic transparent sludge
- Sludge viscosity and peculiar rheology have an important impact on mixing
- PEPT predicted fluid flow near a bubble column more accurately than PIV